NASA Contractor Report 194435

Advanced Technology for a Satellite Multichannel Demultiplexer/Demodulator

Irwin J. Abramovitz, Drew E. Flechsig, and Richard M. Matteis, Jr.
Westinghouse Electric Corporation
Baltimore, Maryland

January 1994

Prepared for
Lewis Research Center
Under Contract NAS–25865

Contents

Advanced Technology for a Satellite Multichannel Demultiplexer/Demodulator

Irwin J. Abramovitz, Drew E. Flechsig, and Richard M. Matteis, Jr.
Westinghouse Electric Corporation
Baltimore, Maryland

January 1994

1.0 Summary

Satellite on-board processing is needed to efficiently service multiple users while at the same time minimizing earth station complexity. The processing satellite receives a wideband uplink at 30 GHz and downconverts it to a suitable Intermediate Frequency. A Multichannel Demultiplexer then separates the composite signal into discrete channels. Each channel is then demodulated by bulk demodulators, with the baseband signals routed to the downlink processor for retransmission to the receiving earth stations. This type of processing circumvents many of the difficulties associated with traditional bent-pipe repeater satellites. Uplink signal distortion and interference are not retransmitted on the downlink. Downlink power can be allocated in accordance with user needs, independent of uplink transmissions. This allows the uplink users to employ different data rates as well as different modulation and coding schemes. In addition, all downlink users have a common frequency standard and symbol clock on the satellite, which is useful for network synchronization in Time Division Multiple Access schemes.

The purpose of this program is to demonstrate the concept of an optically implemented Multichannel Demultiplexer (MCD). A Proof-of-Concept (POC) model has been developed which has the ability to receive a 40 MHz wide composite signal consisting of up to 1000 40 kHz QPSK modulated channels and perform the demultiplexing process. In addition a set of Special Test Equipment (STE) has been configured to evaluate the performance of the POC model.

The optical MCD is realized as an acousto-optic spectrum analyzer utilizing the capability of Bragg cells to perform the required channelization. These Bragg cells receive an optical input from a laser source and an RF input (the signal). The Bragg interaction causes optical output diffractions at angles proportional to the RF input frequency. These discrete diffractions are optically detected and output to individual demodulators for baseband conversion.

Optimization of the MCD design was conducted in order to achieve a compromise between two opposing sources of signal degradation: Adjacent Channel Interference and Intersymbol Interference. The system was also optimized to allow simple, inexpensive ground stations communications with the MCD. These design goals led to the realization of a POC MCD which demonstrates the demultiplexing function with minimal signal degradation.

Performance evaluation results using the STE equipment indicate that the dynamic range of the demultiplexer in the presence of adjacent and multiple channel loading is 40 - 50 dB. Measured Bit Error Rate (BER) probabilities varied from the predicted theoretical results by 1 dB or less.

The performance of the Proof-of-Concept model indicate that the development of a space qualified optically implemented MCD are feasible. The advantages to such an implementation include reduced size, weight and power and increased reliability when compared with electronic approaches. All of these factors are critical to on-board satellite processors.

Further optimization can be conducted which trade ground station complexity and MCD performance to achieve desired system results.

2.0 Introduction

On-board processing is needed to efficiently service multiple users while at the same time minimizing earth station complexity. Figure 2.0-1 is a simplified overview of a satellite communications system that services Frequency Division Multiple Access (FDMA) uplink users. The processing satellite first receives the wideband uplink at 30 GHz and downconverts it to a suitable Intermediate Frequency (IF). A demultiplexer then separates the composite IF signal into assigned channels. All channels are then demodulated by "bulk" demodulators, with the baseband signals being routed to the downlink processor for retransmission to the receiving earth stations via a high-rate Time Division Multiple Access (TDMA) 20 GHz downlink. This type of processing circumvents many of the difficulties associated with bent-pipe repeaters. Uplink signal distortion and interference are not retransmitted on the downlink. Downlink power can be allocated in accordance with user needs, independent of uplink transmissions. This allows the uplink users to employ different data rates as well as different modulation and coding schemes. In addition, all downlink users will then have a common frequency standard and symbol clock on the satellite, which is useful for network synchronization.

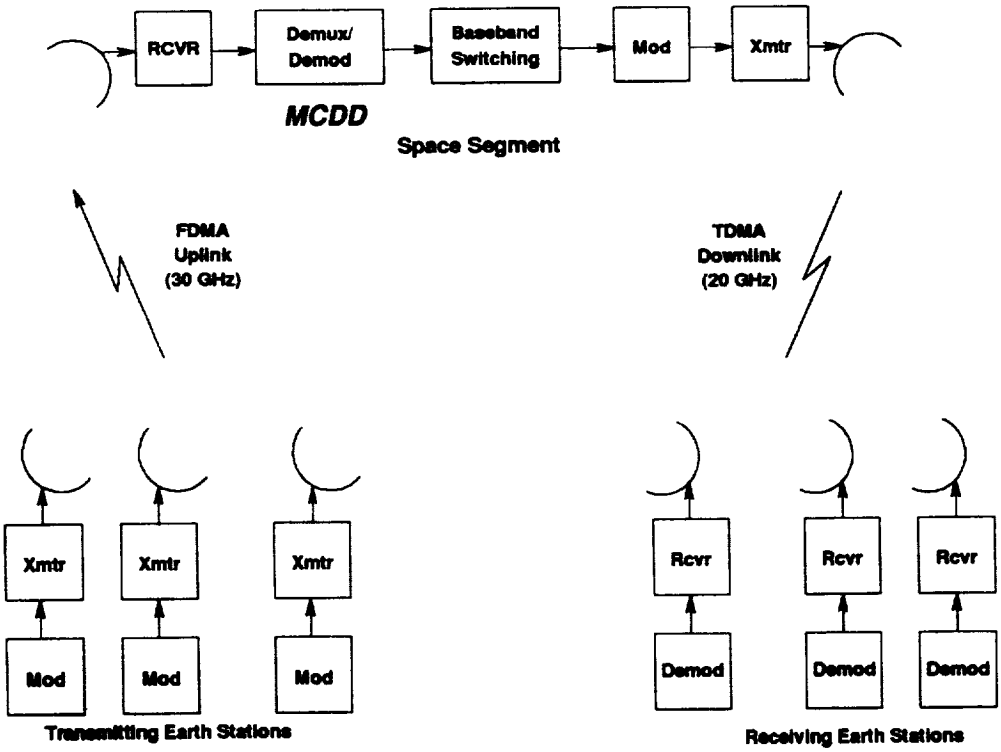

Figure 2.0-1 System Overview

These considerations led to a requirement for on-board multichannel demultiplexer demodulators (MCDD) which can separate and process the individual transmissions with minimal degradation in bit error probability. Implementation of an MCDD is critical because future systems will be highly bandwidth-efficient, which implies very close spacing of the carriers in the composite FDMA uplink.

implementing a wideband A/D conversion on the uplink signal received at the satellite, followed by digital processing that performs the channel filtering and demodulation operations [3]. On-board demultiplexing can also be performed using integrated optics [4,5]. An acousto-optic spectrum analyzer performs both downconversion and channel filtering, with potential savings in hardware size, weight and power and increased reliability.

The following discussion describes how the optical MCDD has been modeled in system performance analyses. Bit error performance is determined in the presence of adjacent channel interference (ACI), intersymbol interference (ISI) and spurious signals generated by the optical processing. The optically implemented Proof of Concept implementation is detailed with a description of system performance evaluation results and recommendations.

3.0 MCDD Development

The MCDD POC development comprised three primary efforts: System Design, POC Fabrication and Test and Evaluation. The details of these efforts are described in the following sections.

3.1 System Design

The MCDD system design comprised three major design tasks. The optical communication system design defined the optical parameters of the POC model including characterization of the space segment and ground segment. The mechanical design realized the optical parameters and resulted in an optically implemented demultiplexer model contained on a single optical baseplate. The Special Test Equipment (STE) design realized a testing environment to evaluate the communications performance of the POC model. The design details for the POC and STE are described in the following sections.

3.1.1 Optical Design

An acousto-optic spectrum analyzer (Figure 3.1-1) employing heterodyne detection can function as a channelized receiver. The spectrum analyzer converts the composite FDMA uplink into acoustic waves in a Bragg cell. These acoustic waves modulate a laser beam, and diffract the beam at angles proportional to the uplink RF signal frequencies. Reference beams are also provided to achieve heterodyne operation, resulting in greater dynamic range. The diffracted light impinges on an array of photodetectors, which function as square-law detectors, and the individual photocurrents are routed to QPSK demodulators. Thus, the acousto-optic spectrum analyzer serves as both a channelizer and downconverter, so that the composite uplink signal is demultiplexed into separate channels, each at a common IF.

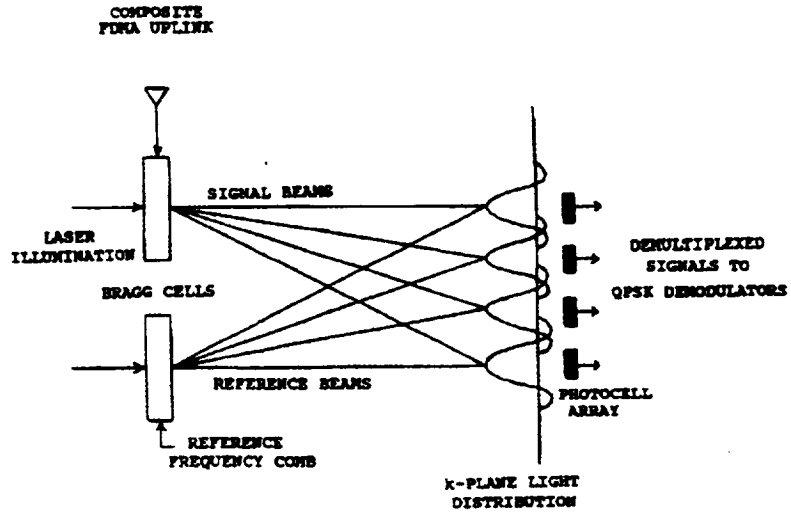

Figure 3.1-1 Acousto-Optic Spectrum Analyzer

To estimate system performance from a demultiplexer of this type, a determination of its transfer function is required. In a classical linear system, a sinusoidal input to the system results in a

sinusoidal output at the same frequency, whose amplitude and phase depend on the frequency. For the heterodyne system considered here, a sinusoidal input results in not only a sinusoidal output at that frequency, but also sinusoids at:

$$f + \sum_n nF, \tag{1}$$

where F is the channel spacing. These spurious sinusoids are generated internal to the demultiplexer by the reference frequency comb (Figure 3.1-2a). In contrast, the frequencies provided by other transmitters external to the demultiplexer make up the ACI (Figure 3.1-2b), which is characteristic of all FDMA systems.

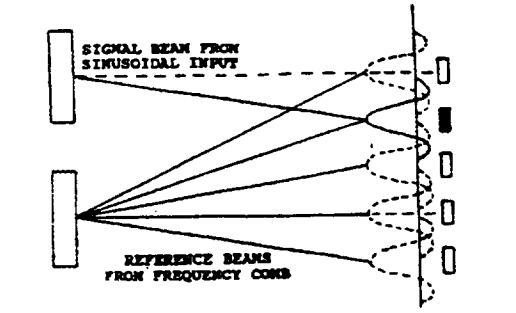

(a) Spurious Signal Distribution from Reference Comb

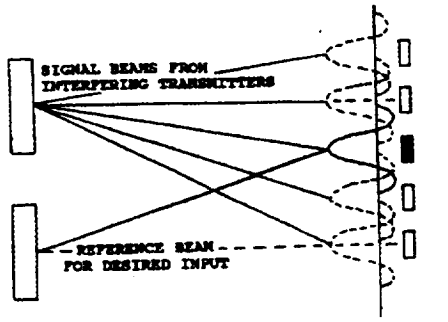

(b) ACI Distribution from Interfering Transmitters

Figure 3.1-2 Interference Effects

3.1.1.1 MCDD Transfer Function

As indicated in Figure 3.1-1, two channels constitute the acousto-optical spectrum analyzer: the "signal" channel and the "reference" channel.

When the beam has a Gaussian cross section, the light into the signal channel Bragg cell can be expressed as:

$$e^{-c_S x^2 + i2\pi f_L t}, \tag{2}$$

where f_L is the light frequency, x denotes distance from the center of the Bragg cell and C_S is a constant determined by the laser beamwidth. This light is modulated by an acoustic wave produced by the input signal channel Bragg cell can be expressed as:

$$e^{i2\pi f_S(t-\frac{x}{v})}, \tag{3}$$

where v is the acoustic velocity in the Bragg cell. Therefore, the modulated light out of the cell is the product of (2) and (3), and the signal channel light distribution in the k-plane is the spatial Fourier transform:

$$F_S(k) = e^{j2\pi(F_L+f_S)t} \int_{-\frac{d_S}{2}}^{\frac{d_S}{2}} e^{-c_S x^2 - i2\pi(\frac{d_S}{v}+k)x} dx, \qquad (4)$$

where d_S is the length of the Bragg cell.

Similarly, the light distribution resulting from the multi-diffracted beam in the reference channel is:

$$F_R(k) = \sum_{n=-\infty}^{\infty} e^{j2\pi(f_L+f_R+nF)t} \int_{-\frac{d_R}{2}}^{\frac{d_R}{2}} e^{-c_R x^2 - i2\pi(\frac{fx+nFy}{v}+k)x} dx, \qquad (5)$$

One of the reference beams is directed toward the signal channel light distribution (4) in the k-plane. However, because the other reference beams also overlap the signal beam to some extent, spurious output signals occur. If a high bandwidth efficiency is required, then the beams must overlap more, which implies a higher level of spurious signals.

The total light intensity in the k-plane is:

$$|F_S + F_R|^2 = |F_S|^2 + |F_R|^2 + 2\mathrm{Re}F_S F_R^*. \qquad (6)$$

By suitably filtering the photodetector output, the only important contribution to the output will be the cross product $G(k)=ReF_SF_R^*$. The photocurrent is proportional to the integral of the intensity over the photosensitive area:

$$I = \int_{k_0-\frac{K}{2}}^{k_0+\frac{K}{2}} G(k)\, dk, \qquad (7)$$

where k_0 is the location of the photocell in the k-plane and K is the width of the photocell. Now let f_0 be the nominal channel carrier frequency, and let $f=f_S-f_0$ represent the input frequency relative to this nominal frequency. Assume that the k-plane location k_0 corresponds to the frequency f_0, so that $k_0 = -f_0/v$. Then the photocell output, translated in frequency to baseband, reduces to

$$I = \sum_{n=-\infty}^{\infty} H_R(f, nF) \cos 2\pi (f - nF)\, t, \qquad (8)$$

where

$$H_R(f, nF) = \int_0^{\frac{D_R}{2}} e^{-c_S x^2} \int_0^{\frac{D_R}{2}} e^{-c_R y^2} \left[\cos\tfrac{2\pi}{v}(fx + nFy) \frac{Sin\,\pi K(x-y)}{x-y} + \right.$$

$$\cos\tfrac{2\pi}{\nu}(fx - nFy)\frac{\sin \pi K(x+y)}{x+y}\Big] dxdy \,. \tag{9}$$

The function $H_R(f,0)$ is the transfer function which will be denoted $H_R(f)$, and which can be calculated by numerical integration after the system parameters have been selected. The terms for which n≠0 give the amplitudes of the spurious sinusoids.

Figure 3.1-3 is the computed transfer function for a particular set of MCDD parameters. The parameters were selected to give the minimum bit error probability in the presence of ACI and ISI when the earth station transmissions are filtered with fifth-order Butterworth filters having time-bandwidth products of 0.5. A bandwidth efficiency of 1.6 bps/Hz has been assumed. We now describe the method used to compute the ACI and ISI. These quantities are needed to determine the transfer function and the bit error probability itself.

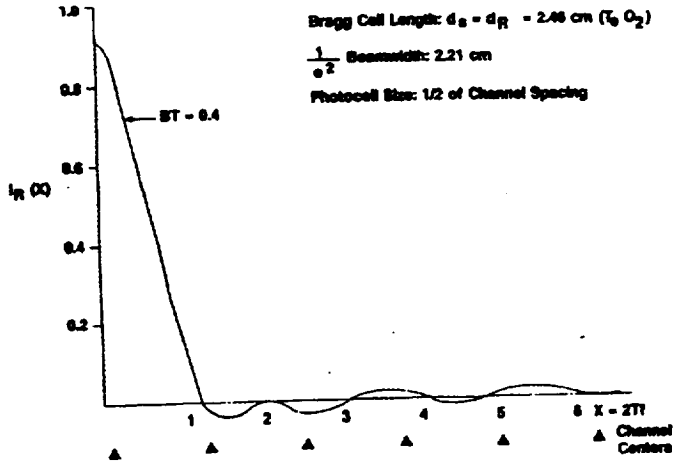

Figure 3.1-3 MCDD Transfer Function

3.1.1.2 Adjacent Channel Interference

Design of any bandwidth-efficient FDMA system involves a fundamental trade-off. If the system bandwidth is narrow, we achieve good ACI performance at the cost of high ISI. Widening the bandwidth reduces the ISI but increases the ACI. The design procedure is generally to select filter types and bandwidths that give the best bit error performance in the presence of both ACI and ISI. We first consider the ACI.

Each ground transmitter is assumed to include bandpass filtering to reduce the amount of ACI entering the satellite receiver (Figure 3.1-4). As a first approximation for performance analysis, the MCDD can be treated conventionally as a bank of bandpass filters, each followed by a demodulator. The model is later generalized to take into account the spurious signals that are characteristic of the MCDD implementation.

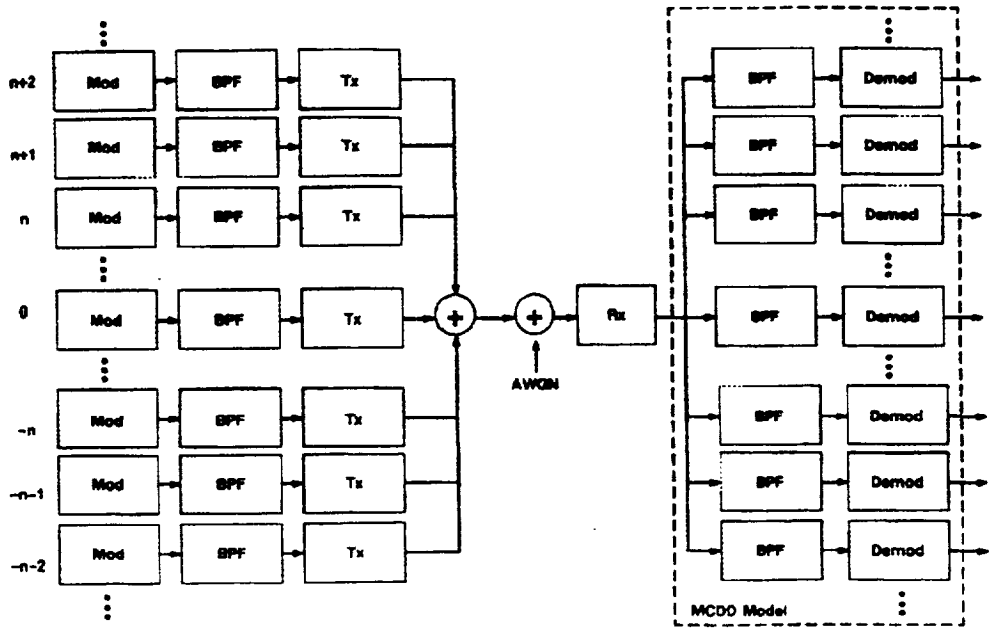

Figure 3.1-4 Analytical Model for Performance Evaluation

It is straightforward to compute the ACI under the assumption that the interference can be treated as noise that adds to the thermal noise at the receiver input. This assumption is valid when there is a large number of interfering users because, according to the central limit theorem, this implies that the interference has nearly Gaussian statistics. We also assume for simplicity that all transmissions arrive at the satellite with equal power, although this is later generalized to include signal fading.

The unfiltered spectral density of the n^{th} QPSK-modulated interfering signal is

$$S(f-nF)=\left[\frac{\sin 2\pi T(f-nF)}{2\pi T(f-nF)}\right]^2. \qquad (10)$$

All ground transmitters have identical filters, and the n^{th} filter transfer function is denoted by $H_T(f-nF)$. Thus the filtered transmission from the n^{th} interferer has a spectral density given by $S(f-nF)\,|H_T(f-nF)|^2$. Suppose the transfer function of the on-board MCDD is $H_R(f)$, which was evaluated in the previous section. Then the spectral density of the interference into the demodulator is

$$\sum_{n\neq 0} S(f-nF)\left|H_T(f-nF)H_R(f)\right|^2. \qquad (11)$$

Assume that the symbol detector is a filter matched to the undistorted symbol (i.e. an integrate-and-dump detector). Its transfer function is $H_{MF}(f) = \sin(2\pi Tf)/(2\pi Tf)$. Then the total ACI power out of the matched filter relative to the undistorted signal power is

$$I = \sum_{n=0}^{\infty} \int_{-\infty}^{\infty} S(f - nF)\left|H_T(f - nF)H_R(f)H_{MF}(f)\right|^2 df. \qquad (12)$$

This is added to the thermal noise to estimate the error probability.

3.1.1.3 Intersymbol Interference

Unlike the ACI, the ISI cannot be approximated as additive Gaussian noise. Instead, we determine explicitly the effect of the transmitter and receiver filtering on the amplitude of the signal out of the integrate-and-dump detector. Expressing any one of the unfiltered QPSK signals before transmission as $s(t) = m(t)\cos(2\pi f_c t + \theta_c)$, the complex modulation is

$$m(t) = \frac{1}{\sqrt{2}} \sum_{n=-\infty}^{\infty} \left[a_n rect\left(\frac{t - 2nT}{2T}\right) + ib_n rect\left(\frac{t - (2n-1)T}{2T}\right)\right], \qquad (13)$$

where a_n and b_n are binary data on the I- and Q- channels respectively, which are assumed to be offset 1/2-symbol. The modulation spectrum of the filtered and demultiplexed signal at the input to its demodulator is

$$\hat{M}(f) = M(f)H_T(f)H_R(f), \qquad (14)$$

where $M(f)$ is the spectrum of the undistorted QPSK modulation. The Fourier transform of this is the distorted modulation, which we will call $\hat{m}(t)$, and the output of the I-channel integrate-and-dump detector in the demodulator is

$$\frac{1}{2T}\int_{-T+\tau}^{T+\tau} \hat{m}(t)dt = T\sum_{n=0}^{\infty} a_{-n} \int_{-\infty}^{\infty} H_T(f)H_R(f)\left(\frac{\sin 2\pi Tf}{2\pi Tf}\right)^2 e^{i2\pi(2nT+\tau)f} df, \qquad (15)$$

where τ is the sampling time relative to the symbol transition. The Q-channel output is similar. Because the filters introduce group delay, the sampling time is generally nonzero. We can split the composite transfer function $H_T(f)H_R(f)$ into its real and imaginary parts denoted by $\alpha(f)$ and $\beta(f)$ respectively. Because α is an even function of f and β is odd, the signal amplitude out of the I-channel of the detector becomes

$$S = 2\sum_{n=0}^{\infty} a_{-n} \int_{0}^{\infty} \left(\frac{\sin \pi x}{\pi x}\right)^2 \left[\alpha(x)\cos 2\pi\left(n + \tfrac{\tau}{2T}\right)x - \beta(x)\sin 2\pi\left(n + \tfrac{\tau}{2T}\right)x\right] dx, \qquad (16)$$

after changing the integration variable. This shows that the detector output includes contributions from not only the desired (n=0) symbol, but from all symbols, which is what is meant by intersymbol interference. The bit error probability can be estimated from either the I-channel or Q-channel output.

By differentiation, we find that the value of τ for which the average value of S is a maximum is the

solution of

$$\int_0^\infty \left(\frac{\sin x}{x}\right)^2 \left[\alpha(x)\sin\frac{\pi x}{T} + \beta(x)\cos\frac{\pi x}{T}\right]dx = 0. \qquad (17)$$

Once the optimum τ is found we can compute the contribution to S from the n=0 symbol and from all important interfering symbols. It has been found that the n = 1,2,3, and -1 interfering symbols are the significant contributors in this application.

The bit error probability is then computed by averaging the error probability, conditioned on a particular sequence of the interfering symbols, over all 16 possible sequences of these symbols. The noise in this computation consists of the ACI, which was calculated in the previous section, plus the thermal noise at the input to the satellite receiver. If N_0 is the thermal noise density at the input, the thermal noise power at the output of the integrate-and-dump detector is

$$N_0 \int_{-\infty}^{\infty} |H_R(f)_{MF}(f)|^2 df, \qquad (18)$$

which is added to the ACI in the error probability computation.

3.1.1.4 MCDD System Design Results

Having derived the MCDD transfer function, and having calculated the ACI and ISI, it is straightforward to express the total power out of the device as

$$P = \sum_n \sum_m \int_{-\infty}^{\infty} S(f - nF)\left|H_T(f - nF)H_R(f, mF)H_{MF}(f)\right|^2 df. \qquad (19)$$

The first sum is over the number of interfering earth stations, while the second is over the number of spurious signals produced by the reference beams. The m=n=0 term is the desired output; the m=0, $n\neq$0 terms are the ACI; the $m\neq$0, n=0 terms are the spurious outputs when there is only one uplink signal; and the $m\neq$0, $n\neq$0 terms are additional spurious outputs arising from interaction of the interfering channels with the $n\neq$0 reference beams. Of this latter category, the m=n terms dominate, and are therefore included in the performance calculation. The m=n interaction terms are illustrated in Figure 3.1-1, while the $m\neq n$ terms are illustrated in Figure 3.1-2.

Figure 3.1-5 shows the bit error probability when the MCDD transfer function is that shown in Figure 3.1-3. Fifth-order Butterworth filters are used in the earth station transmitters, and integrate-and-dump symbol detection is assumed. The effects of ACI, spurious signals, and ISI are all included in the calculation. Also shown for comparison is a case where the optical MCDD is replaced by a bank of bandpass fifth-order Butterworth filters whose bandwidths are optimized to give the smallest bit error probability in the presence of the same interference. Figure 3.1-5 shows that the performance of an optical MCDD compares favorably with that of an MCDD implemented electronically.

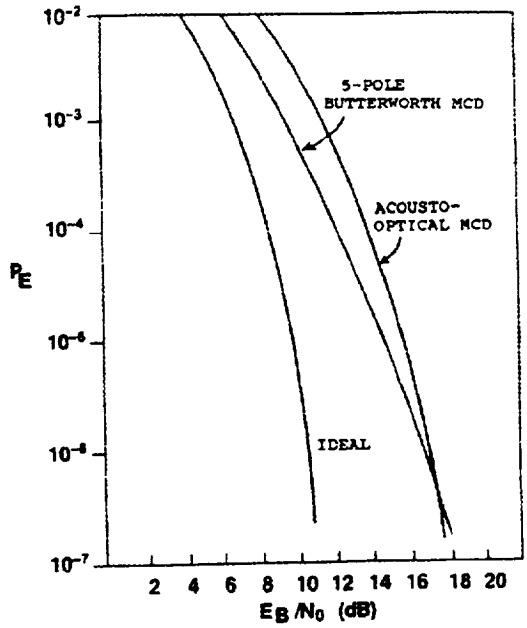

Figure 3.1-5 Bit Error Probability

Figure 3.1-6 shows the sensitivity of system performance to timing errors in the symbol detection circuitry. This is evaluated by varying the sampling time about its optimum value when computing the error probability. It is evident that when the timing error is less than approximately ten percent of the symbol duration, its contribution to bit error degradation is insignificant compared to the ACI, spurious signals and ISI.

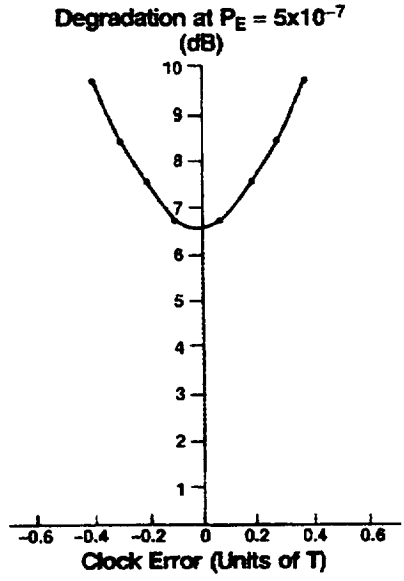

Figure 3.1-6 Sensitivity to Symbol Synchronization Error

3.1.1.5 Signal Fading

The MCDD POC model parameters have been optimized to achieve the best bit error performance in the presence of an eight dB rain fade. It is these optimized parameters that were used to compute the MCDD transfer function of Figure 3.1-4.

Table 3.1-1 lists the optimum MCDD parameters computed under the condition of no fading and under the condition of an eight dB rain fade. Fading was modeled by an increase in the adjacent channel interference. The POC model parameters have been chosen for optimum performance in the presence of an eight dB fade, which corresponds to the column denoted B in the table. Figure 3.1-7 shows the bit error curves for the conditions listed in Table 3.1.1.5-1. Curve B is the expected performance with an eight dB fade.

Table 3.1-1 Optimum MCDD Parameters With and Without Fade

Curve A: MCDD parameters optimized for no fade. Performance is with no fade.
Curve B: MCDD parameters optimized for 8dB fade. Performance is with 8 dB fade.
Curve C: Compromise parameters. Performance is with 8 dB fade.
Curve D: MCDD parameters optimized for 8 dB fade. Performance is with no fade.
Curve E: MCDD parameters optimized for no fade. Performance is with 8 dB fade.

*d=Bragg cell length. BW=laser beamwidth. K/Δk=ratio of photocell size to photocell spacing in k-plane. Degradation is evaluated at $P_E=5x10^{-7}$.

MCDD Parameters*	A. & E.	B. & D.	C.
d_S	2.33 cm	2.45 cm	2.39 cm
d_R	1.87 cm	2.21 cm	2.03 cm
BW_S	2.10 cm	2.21 cm	2.15 cm
BW_R	1.68 cm	1.99 cm	1.83 cm
K/Δk	0.48	0.48	0.48
Degradation	5.4 dB and > 10 dB	7.1 dB and 5.4 dB	9.8 dB

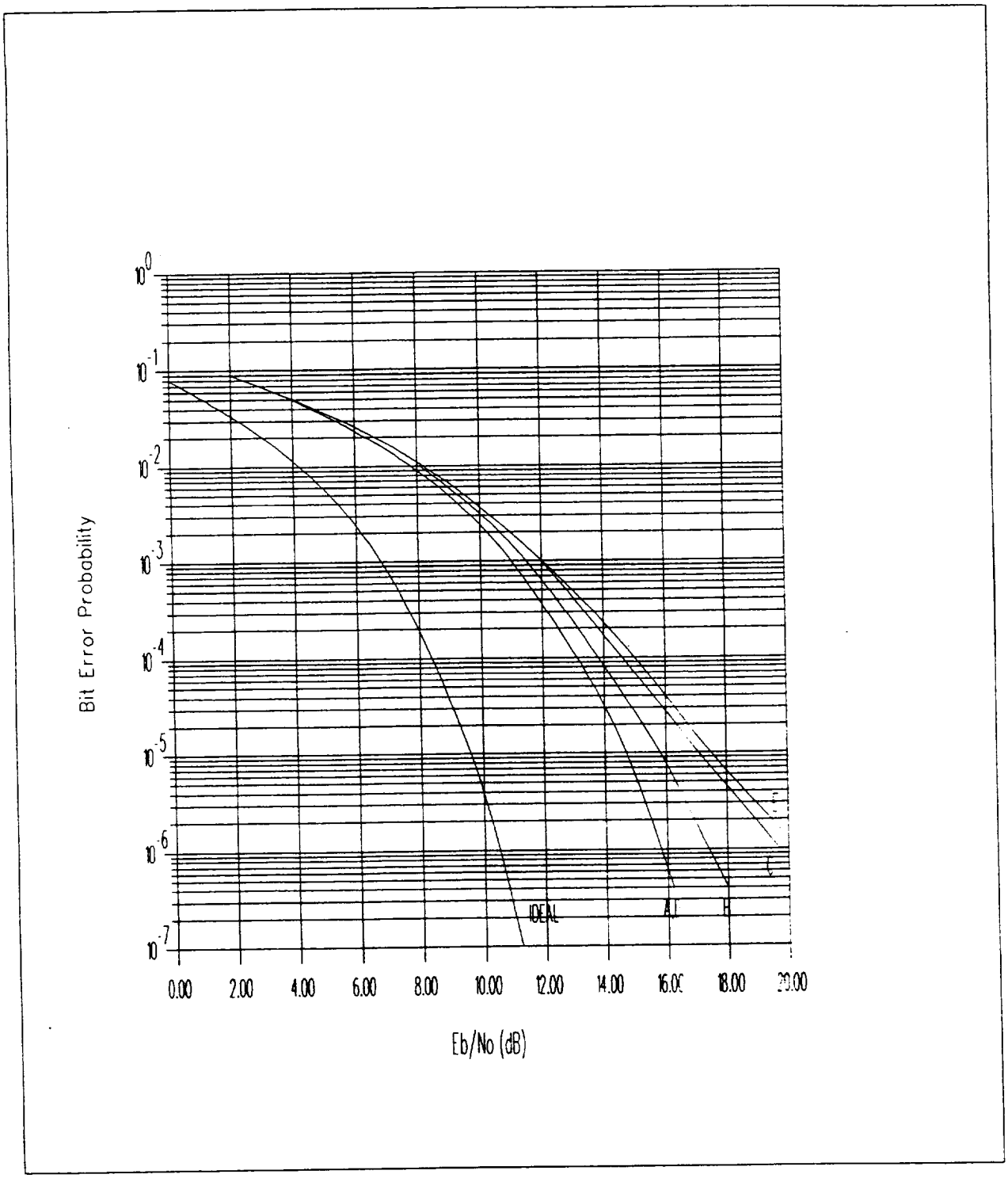

Figure 3.1-7 MCDD Theoretical Performance With and Without 8 dB Rain Fade

3.1.1.6 Ground Transmitter Filters for MCDD

During STE design, it was found that five-pole Butterworth filters were not available at the required frequency for the STE developed to test the POC model. Therefore, the expected system performance is examined when four- and six-pole Butterworth filters are used instead.

To do the analysis without changing POC model design, those parameters that have been optimized for five-pole Butterworth transmitter filters were retained, as summarized in Table 3.1-2.

Table 3.1-2 MCDD Parameters

Signal aperture	2.45 cm
Reference aperture	2.21 cm
Signal beamwidth	2.21 cm
Reference beamwidth	1.99 cm
PD size-to-spacing ratio	0.48

Table 3.1-3 summarizes bit error performance for the three transmitter filter types. Note that the bandwidth of the six-pole filter must be somewhat larger than that for the other filters, in order to achieve optimum performance. Of course better performance can be achieved by re-optimizing the MCDD parameters as well.

Table 3.1-3 Bit Error Performance

No. of Poles	BT	No Fade	8 dB Fade
4	0.5	6.3	9.6
5	0.5	5.4	7.1
6	0.55	5.4	7.3

3.1.2 Mechanical Design

The following sections describe the mechanical engineering design of the MCDD POC model. This design comprises the optical baseplate, optics and mounts required to realize the POC model.

3.1.2.1 Mechanical Design Overview

The goals in the mechanical packaging of the MCDD POC are to demonstrate both the functionality of an optically-based processing system and packaging suitable for satellite systems. In these two aims, a compact, flat system was designed and built so that all subsystems are accessible and reconfigurable into a smaller package. This technology demonstrator could have been built utilizing a large optical bench and standard optical mounts, however, this approach would display none of the packaging considerations crucial for future satellite implementations.

3.1.2.2 Design Requirements

The major mechanical design requirements deal with the mounting of optical components. Off-the-shelf optics are used wherever practical, however for certain subsystems, only custom optics are suitable. The packaging revolves around passing a laser beam through acousto-optic Bragg cells within interferometers while providing prescribed beamwidths through the cells. A collimated laser source is expanded with prisms, and fed through the interferometer and telescope optics to a detector. In this way, the POC is divided into six primary subassemblies: laser source, prism expander, interferometer, output optics, detector, and base/chassis. Each subassembly is designed for access in a bench-top environment as depicted in Figure 3.1-8.

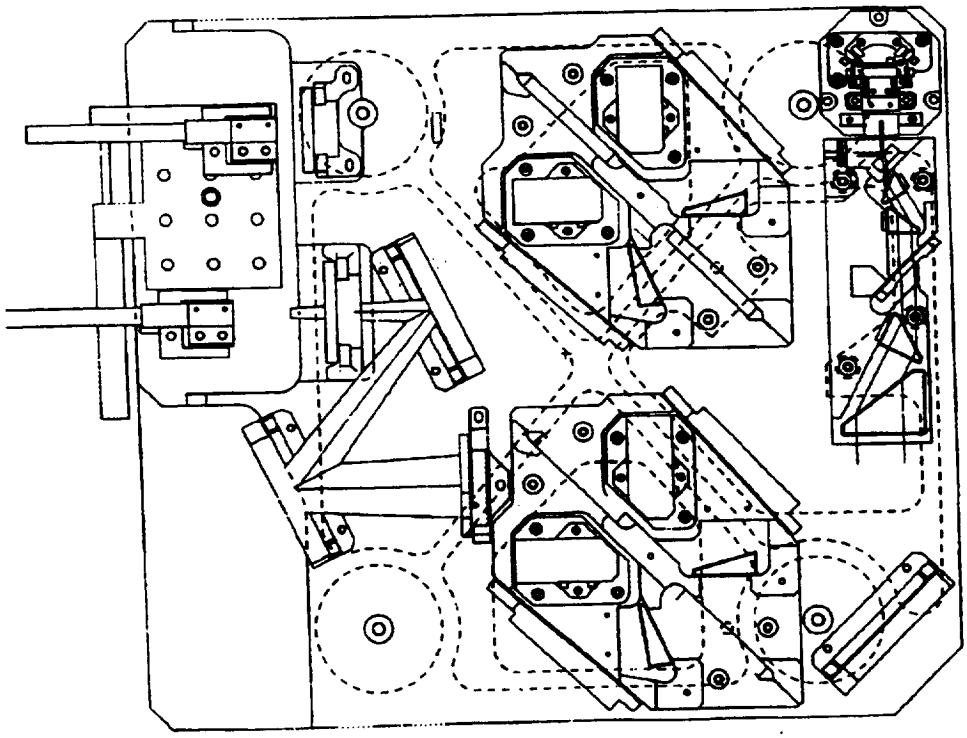

Figure 3.1-8 MCDD POC Optical Baseplate Layout

Each subassembly is aligned individually so that the permutations of adjustments are minimized.

Wherever possible, optical elements are fixed, so that the most sensitive element can act as the adjustment mechanism.

The primary construction material for the system is 6061-T6, the most stable and readily available aerospace aluminum. For the interferometers, a stainless steel with a Coefficient of Thermal Expansion (CTE) much lower than that of the 6061-T6 is utilized, owing to the higher relative stability required of that subassembly. Aluminum is suitable for most of the system because of its low cost and density, and the benign environment expected within the laboratory. For production systems, other materials should be considered, such as composites, for lower weight, greater stability and lower CTE.

3.1.2.2.1 Laser Source Subassembly

The Laser Source subassembly produces the collimated IR laser beam used to demultiplex the incoming RF signals. The subassembly houses four optical components: a Mitsubishi ML-5415N-01 Laser Diode, a Kodak A-365-D Aspheric Lens for collimation, a Special Optics Half Wave Plate for polarization and an interference filter. The subassembly is designed so that optical elements can be aligned prior to system assembly. The structure supporting these elements is made from 6061-T6 aluminum which provides sufficient thermal and structural stability to maintain optical alignment in the laboratory environment.

The major mechanical design requirements for laser source subassembly deal with optical alignment of the laser diode and collimating lens and temperature control of the laser diode. These requirements are listed in Table 3.1-4 below.

Table 3.1-4 Laser Source Assembly Requirements

Thermal Requirements	
Laser Diode Temperature Tolerance:	+/- 1.0 degree
Heat Sink Dissipation:	6.5 watts
Laser Diode to Collimating Lens Alignment Tolerances	
Focus (X axis translation):	+/- 0.001 inches
Decentering (Y and Z axis translations):	+/- 0.001 inches
Gaussian (Z axis rotation):	+/- 0.1 degrees
Beam Spread Orientation (X axis rotation):	+/- 2.0 degrees

The subassembly consists of three support structures mounted on a common base. One structure houses the laser diode, the second contains the collimating lens and half wave plate and the third supports the interference filter. An exploded view of these structures is shown in Figure 3.1-9. The laser diode support structure provides three rotational and two (Y and Z axis) translational degrees of freedom for optical alignment as well as a thermal electric device (TED) and thermistor for temperature control. The collimating lens structure provides X axis translation for focusing the lens.

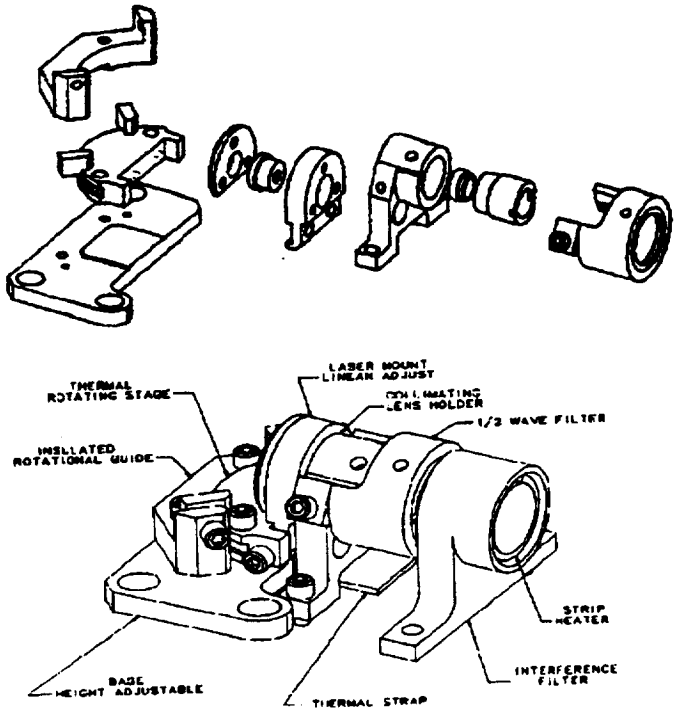

Figure 3.1-9 Laser Source Subassembly

The laser diode support structure was designed to minimize coupling between the adjustments while maintaining a good thermal path from the diode to the heatsink. To ensure sufficient heat flow, the diode is coated with thermal grease and positioned in an aluminum housing. The diode can be rotated in this housing to provide the desired beam spread direction. A retaining plate presses the diode against the housing to establish a thermal path. A thermistor is also mounted in the housing near the diode to monitor its temperature. The housing is bolted to a rotational plate. The interface between these parts incorporates opposing adjustments screws which provide controlled linear translation along the Y axis.

The rotational plate is positioned by a guide which provides rotational adjustment of the diode about the Z axis by way of opposing screws, and sits on top of a Melcor thermal electric device (TED). The rotational guide is locked into position by two nylon screws which are screwed into a baseplate under the TED. This arrangement places the TED in compression ensuring a good thermal interface. The rotation guide is a made from epoxy glass to prevent thermal short-circuiting of the TED.

The baseplate provides the remaining adjustments for the laser diode. The plate is mounted to the laser subassembly base with three lockable, adjusting screws which provide rotation about the Y axis and translation in the Z axis direction. The baseplate has been nickel plated with a braided copper thermal strap soldered to it. The thermal path is completed by the other end of the strap to the optical baseplate.

The collimating lens and interference filter structures are simpler than the laser diode structure.

The collimating lens structures require only a focusing adjustment and the filter structure is a simple mount. This is accomplished by loading the lens into an aluminum lens cell which has a flange and threads on the exterior. The lens cell screws into the lens base along the optical axis to focus the lens. Once the lens has been focused the cell is locked into position with set screws. The half wave plate does not require precise alignment and is mounted into an aluminum housing and bolted to the lens base.

3.1.2.2.2 Expander Assembly

The expander assembly expands the collimated laser beam to the prescribed beamwidths for both the narrowband and wideband interferometers. This is accomplished by performing a two stage expansion of the beam. First, the beam is expanded by two prisms to the input beamwidth for the wideband interferometer. The beam is then split using a 50% reflective / 50% transmissive beam splitter. The reflected beam enters the wideband interferometer while the transmitted beam is expanded by two more prisms to achieve the prescribed narrowband beamwidth.

All of the expansion optics are mounted on a common base. Since the optics are not sensitive to alignment, each prism is simply pressed against a reference surface in the expander base and epoxied into position. The beam splitter is glued into a stainless steel frame and attached to the base with lockable adjusting screws.

A laser beam pick-off is used to monitor the output of the laser for shifts in wavelength or power output. The pick-off is a beam splitter which has 2% reflectance and 98% transmission. The reflected beam is then measured by a photodiode which is mounted on the side of the expander base. This pick-off is designed, but not integrated into the current POC configuration.

3.1.2.2.3 Interferometers

The interferometers for the wideband and narrowband channels are built of the same basic design, with only minor differences between the two. It is therefore only necessary to detail the design of one and describe the differences of the other. For the purposes of this report, the narrowband interferometer is described in detail, as this was the most challenging channel to build, and was the basis for the design of the wideband channel.

The interferometer design is based on a Michelson interferometer. This type of interferometer was originally intended for the study of materials with different indices of refraction. A material of one index is placed in one arm of the interferometer, and a second of another index is placed in the other arm. In this way, one material acts as a reference for comparison to another. This is exactly what is done in the MCDD interferometers.

The MCDD interferometers contain a Tellurium Dioxide (TeO_2) acousto-optic Bragg cell in each arm. These cells, as they are driven by RF inputs to a transducer located on one end, set up acoustic waves within the crystalline structure, changing its index of refraction. The input beam is split into three beams. The main beam continues through the crystal subject only to the refraction of the ordinary crystal, and two beams are refracted with some slight angular change based upon the acoustic signal within the crystal. This angular change is directly proportional to the frequency of the acoustic wave, which is in turn, directly proportional to the RF input. Each of

these refracted beams exit the acousto-optic crystal at ± a delta angle with respect to the main beam, but at polarizations that are 90 degrees out of phase with each other. One of these polarizations is stronger and more stable than the other, and is used for signal processing.

The arms of the interferometer are required to be of similar length. For packaging reasons resulting from a design goal of producing a compact system, the arms are not just equalized, but minimized. The overall beamwidth becomes the limiting value in sizing the interferometer. For signal interference optimization, two beamwidths are required, a narrower beam through the reference Bragg cell, and a wider beam through the signal Bragg cell. In order to provide cost savings through greater part commonality, the beam input was established as an intermediate width, so that identical prisms could be utilized to expand and contract the beam to go through the appropriate Bragg cells. The splitter and combiner are of the same design, as are the corner mirrors. The corner mirror mounts are designed as left- and right-handed pairs. As the diffracted angle is different for the wideband and narrowband interferometers, the angle of the side of the interferometers is set to the lowest value, and the mirror holders are designed to compensate for the difference.

3.1.2.2.3.1 Bragg Cells

The Bragg cells are TeO_2, an orthotropic material. The CTE in the crystalline directions is different, thus requiring a close match of the Bragg cell base to the long direction of the crystal to minimize stress. The most readily available material which most closely matches the CTE of TeO_2 is free-cutting brass. The base of the crystal housing was made of brass, and the crystal was bonded to it with RTV. The brass was blackened to reduce the amount of reflected radiation. The crystal base has a cylinder machined in its bottom which matches a hole in a second brass piece that is mounted to the interferometer by way of three lockable, adjusting screws. In this way, each Bragg cell has three rotational and one translational degrees of freedom.

3.1.2.2.3.2 Interferometer Base

In order to prevent thermoelastic deformations of a magnitude to disrupt signal processing, the CTE of the base is required to be low. At the same time the desire is to have high thermal conductivity to prevent thermal gradients from being established, which could lead to distortion. Because no readily available, low-cost material can meet both requirements, selection was based primarily on low CTE with the understanding that the device is to be used in a laboratory environment where thermal control can easily be maintained. The material selected for the base was 416 series stainless steel. This particular material is readily available and machinable.

Follow-on designs should take advantage of engineered materials, such as metal matrix composites which combine low CTEs and high thermal conductivity in a machinable form. These composites also offer the advantage of relatively low densities and high strength and moduli.

3.1.2.2.3.3 Optics

All optics are made of BK-7 glass. The prisms are AR coated and optimized for the given input angles. The mirrors and beam splitters all use the same size blanks. The mirrors are given

reflective gold coatings, and the splitters are given AR coats optimized for 45° incidence. The prisms all have AR coatings designed for their particular angle of incidence.

3.1.2.2.3.4 Detector

The detector is a single Motorola MFOD 1100 photodetector. It is mounted to two orthogonal translation stages. The translation stages are Newport equipment. One short range stage is used for final focusing and a large stage is used for translating the detector across the image (signal) plane, so that a single detector can be used to sample any channel. As a result, precise measurements of crosstalk and signal strength are possible. The single detector is used to minimize cost, while providing a very testable system.

3.1.2.2.3.5 Base

The base is constructed of aluminum and anodized black. It is designed to fit within an ordinary electronics rack on small vibration isolators. A sheet aluminum and plexiglass cover fits over the base to protect it from dust. All mounting features, for the components, are machined into the base.

3.2 Narrowband POC Fabrication

The following sections describe the fabrication process for the POC model. Included in the description is a characterization of the optical components and procedure for optical alignment.

3.2.1 Component Characterization

3.2.1.1 Laser Diodes

The laser diode selected for this application is a Mitsubishi ML-5415N-01 GaAlAs Fabry-Perot laser with emission wavelength near 8200 angstroms and maximum output power of 30 milliwatts. This laser is a new model which replaces the ML-5702A used successfully in other Westinghouse optical processors. The emission spectra of the laser is predominantly single frequency at drive currents above threshold. The laser supports a single longitudinal and transverse mode which exhibits a Gaussian beam profile essential for low sidelobes and high channel isolation.

In order to ensure reliable device operation, two lasers with room temperature emission wavelengths of 820 nanometers were burned in for over 200 hours at peak output power. During the burn-in period the laser emission spectra was monitored on a spectrophotometer to ensure stable, single-frequency operation. The typical laser spectrum for a drive current of 120 milliamps, shown in Figure 3.2-1, illustrates the single-mode characteristics of the laser source.

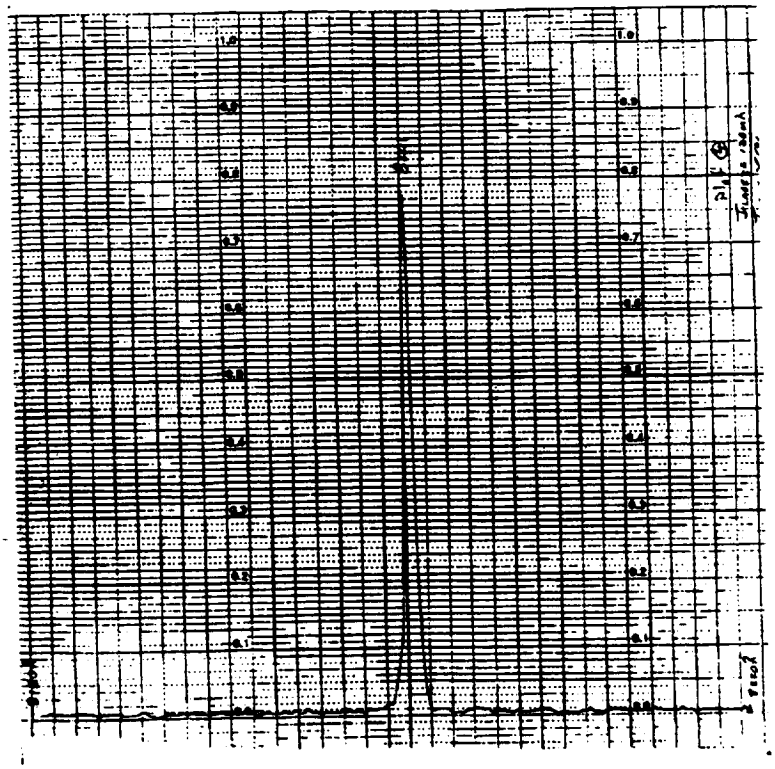

Figure 3.2-1 Mitsubishi ML-5415N-01 Single-Mode Characteristics

The emitted laser power is controlled by the forward diode current and follows a linear relationship above the threshold. The current dependence of the laser power is measured with a calibrated optical power meter and is displayed in Figure 3.2-2. With a forward current of 120 milliamps the laser emits 20.8 milliwatts of optical power out of the front facet of the device. The lasers selected for this application incorporate a photodiode in the laser diode can which intercepts the laser emission out of the rear facet and provides an output signal proportional to the emitted power. These monitor photodiodes are convenient for determining the laser status in source assemblies where the laser path is not readily accessible.

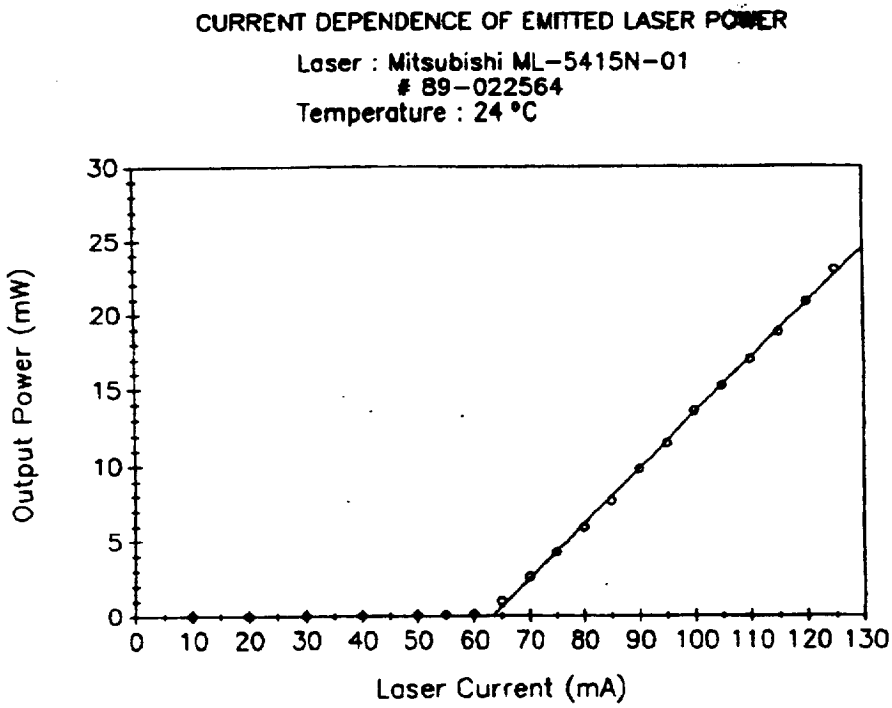

Figure 3.2-2 Laser Current vs. Output Power

The laser diode is susceptible to damage caused by electro-static discharge (ESD) and reverse bias voltages exceeding three volts. Proper ESD procedures, including grounding to prevent static charge accumulation, are recommended when the device is removed from the circuit. It is also strongly recommended that the laser diode connections be isolated from earth ground to prevent device failure. During the initial device characterization, one laser diode failure was observed due to improper ground isolation which is described in detail in Section 3.3.5.3.

3.2.1.2 Optical Interference Filter

The MCDD POC demultiplexer is a coherent channelizer which utilizes the Bragg acousto-optic interaction to separate channels according to their carrier frequency. Since the acousto-optic interaction is also a function of the laser wavelength, stable frequency channelization requires control of the laser wavelength. A narrow bandpass optical filter provides a convenient

mechanism for sensing small wavelength shifts. By monitoring the changes in transmitted optical power and using these feedback signals to control the temperature of the laser diode, the emission wavelength of the optical source can be maintained within a small range. However, this form of feedback control was not implemented in the current POC configuration. It is recommended that a feedback mechanism be implemented in future systems to ensure laser stability.

The interference filter for the POC is designed to exhibit a 4.5 angstrom full-width, half-maximum bandpass with a center wavelength near 8200 angstroms. The peak transmission is 50% and the system is designed for normal incidence.

To verify the filter characteristics, the laser diode temperature was adjusted until the wavelength was near the center of the filter passband and laser radiation was transmitted through the device. However, when the optical insertion loss of the filter was determined by measuring the incident and transmitted power, a peak transmittance of 23% was observed in contrast to the 50% value measured by the vendor. A more accurate measurement of the filter passband was performed using the spectrophotometer and the result is displayed in Figure 3.2-3. The spectral response is consistent with the measurement and confirms the lower peak transmittance of 23%.

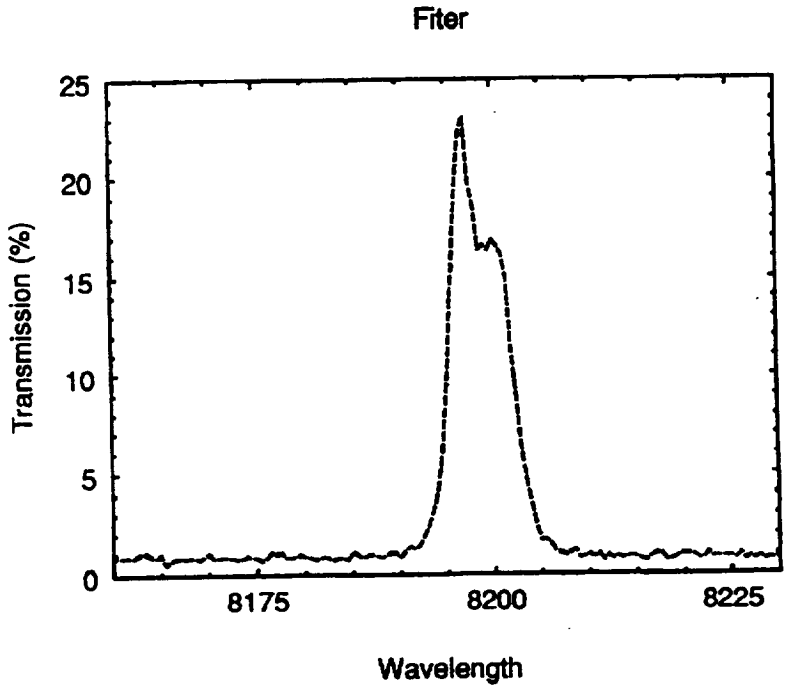

Figure 3.2-3 Spectrophotometer Measurement of Filter Characteristic

Subsequently, both interference filters were returned to the manufacturer for characterization. Andover concluded that the filters were not aged properly, resulting in a shift in the center wavelength and a decrease in the peak transmittance. Since the degradation in the filter performance was due to a manufacturing error, the vendors fabricated two new filters at no cost to the program. The manufacturer's spectral response plot for one of the filters is presented in

Figure 3.2-4. The delay in receiving the new filter did not allow sufficient time to verify the manufacturer's measurements.

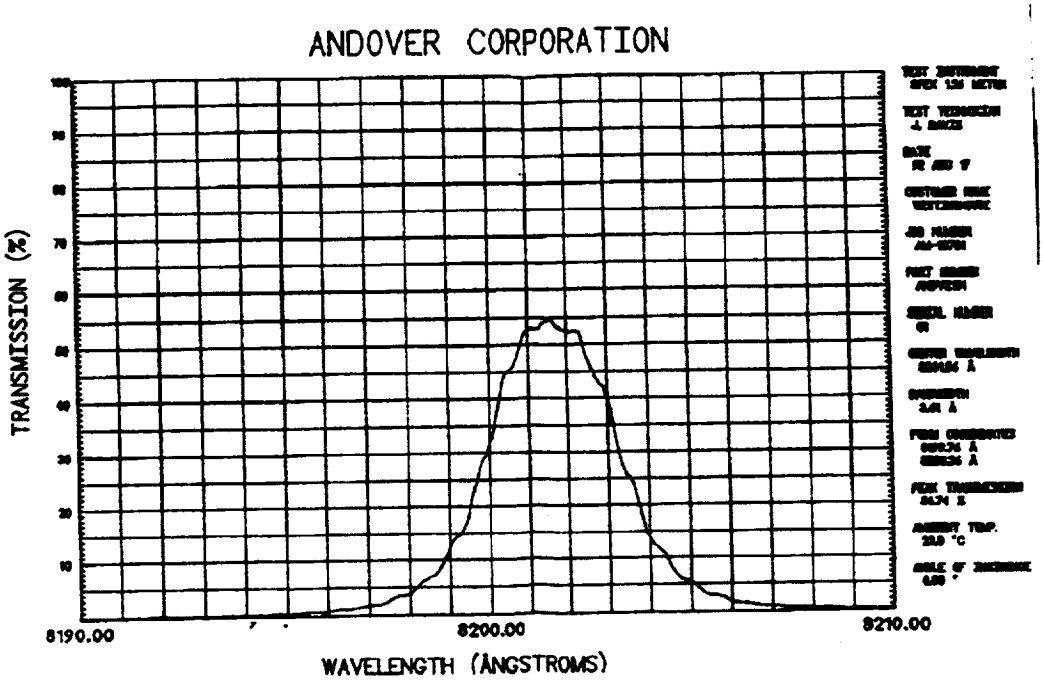

Figure 3.2-4 Filter Spectral Response

3.2.1.3 Mirrors, Beam Splitters, and Expanders

Other critical system components include the mirrors, beam splitters and the anamorphic beam expander. The characterization of these elements entails measuring the incident, reflected and transmitted power for polarizations parallel and perpendicular to the plane of incidence at the specified angle of incidence.

To evaluate the coatings deposited on these components, the output from a laser diode with an emission wavelength near 8200 angstroms was collimated and passed through a polarization rotator. The rotator allows the polarization vector of a linearly polarized incident beam to be aligned along any arbitrary direction. The linearly polarized output illuminates the facet of an element under test. To align the beam at the specified angle of incidence, the component is mounted on a precision rotary table. Normal incidence is achieved by rotating the table until the reflected and incident beams are collinear. With the normal position established, the proper angle of incidence is achieved by rotating the table through an angle equal to the specified angle of incidence.

All of the coatings on the mirrors and beam splitters were evaluated at an angle of incidence of 45°. The measurements were performed with the proper polarization orientation and resulted in data which is consistent with the design specifications.

The anamorphic beam expander consists of four cascaded right-angle prisms positioned such that the angle of incidence is approximately 65° and the exit angle is 0° relative to the normal for each of the prisms. The prism anti-reflection coatings are designed for a vertical polarization vector, i.e. perpendicular to the plane of incidence. The ratio of the reflected and incident power for these coatings is less than or equal to 1% which is consistent with the design specifications.

3.2.1.4 Bragg Cells

The Bragg cells used in the narrowband processor are TeO_2 slow shear crystals operating over the 50 MHz to 90 MHz frequency band with a nominal optical aperture of 2 mm (H) x 24 mm (W). Due to the attenuation of the acoustic wave in the cell, the diffraction efficiency is dependent upon the proximity of the optical beam to the transducer. To characterize the cell, the diffraction efficiency near the center frequency of the RF band is measured with the laser waist positioned at the limits of the optical aperture. The maximum diffraction efficiency occurs when the laser spot is near the acoustic transducer, while the minimum diffraction is observed when the optical beam is at the far end of the cell. This measurement defines the limits of the diffraction efficiency across the useful aperture of the device.

The measurement system for characterizing the acousto-optic cells is similar to the setup used for verifying the mirror and beam splitter performance. An infrared objective is aligned in front of a laser diode with an emission wavelength near 8200 angstroms so that a laser waist is formed in the center of the Bragg cell. In order to facilitate the measurements, the Bragg cells are positioned on a precision rotary table to allow optimization of the Bragg angle. The diffraction efficiency, which is the ratio of the optical power in the first diffraction order and the incident optical power, is measured with 50 milliwatts of RF power applied to the cell. Linear extrapolation is used to express the diffraction efficiency in units of percent/Watt.

The minimum diffraction efficiency measured for the narrowband Bragg cells 3809 and 3810 are 125%/Watt and 90%/Watt, respectively. These values are in agreement with the specifications supplied by the manufacturer, Crystal Technologies.

While the cells are aligned on the test fixture, the relative diffraction efficiency across the 40 MHz bandwidth is observed by viewing the first diffraction order with an infrared viewer as the RF is swept from 50 MHz to 90 MHz. A uniform intensity was observed across the band.

The cells were also visually inspected by viewing between crossed polarizers to detect strains in the crystal. No apparent strains were detected.

During final system testing a failure in the signal Bragg cell was detected. The Bragg cell failure was caused by a delamination of the acousto-optic transducer from the cell. This delamination is a manufacturing defect. The loss of contact between the transducer and the cell manifested itself as a glitch causing a loss in diffraction efficiency. The failed MCDD Bragg cell had a glitch at 70.0 MHz as higher power was applied to the cell. The manufacturer indicates that this problem is atypical of this type of cell and in a production lot extended RF burn-in can eliminate infant mortality and increase the reliability of the cells. The manufacturer also indicated that similar

Bragg Cells in production lots are not exhibiting this delamination which may have been caused by contamination in the chamber used in the manufacturing process. The manufacturer replaced the faulty cell without additional cost to the program.

3.2.2 Alignment and Assembly

3.2.2.1 Laser Source Assembly

The laser source assembly, illustrated in Figure 3.2-5, consists of two sections: the laser subassembly and the anamorphic beam expander. The laser and collimating optics are mounted on a detachable baseplate that allows the laser subassembly to be removed to facilitate beam alignment and diagnostics. The laser subassembly, Figure 3.1-9, consists of a Peltier thermoelectric device with thermistor for controlling the laser temperature and wavelength, a laser diode with integrated monitor photodiode, an aspheric collimating lens, a half-wave plate for setting the laser polarization and a narrow passband optical interference filter. The mechanical mounts for these components are described in Section 3.1.2.2.1.

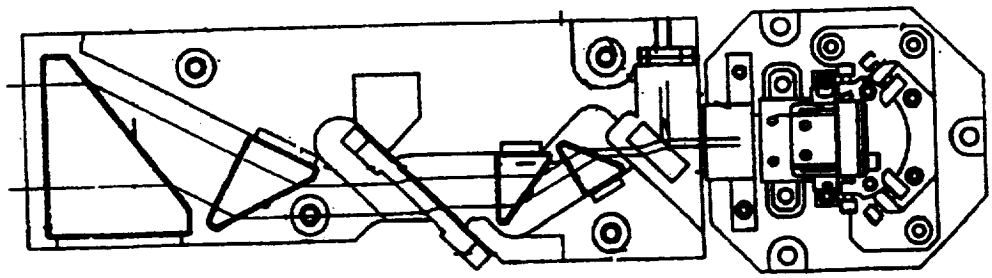

Figure 3.2-5 Laser Source Assembly

The beam expander subassembly is mounted on a separate baseplate, as illustrated in Figure 3.1-8. The collimated beam at the input of the beam expander subassembly is incident on a pick-off mirror which reflects a small percentage of the light onto a photodetector. The output from this detector provides a feedback signal which is used to control the laser temperature and maintain the emission wavelength in the center of the interference filter passband. The light which passes through the pick-off mirror is expanded in the transverse dimension as it propagates through the first two beam-expansion prisms. Provisions have been made to insert a beam splitter at this point in the beam expansion subassembly to direct half of the laser power to the wideband interferometer. Since the wideband processor is not implemented in the current POC configuration, this beam splitter is not currently installed in the system. Consequently, all of the light passes through the final two beam expansion prisms and into the narrowband interferometer.

To achieve the desired system performance, the laser source must be properly aligned which entails collimating the laser and adjusting the beam propagation direction. Both of these alignment procedures are performed with the laser diode subassembly positioned on an optical table. The laser is initially aligned by observing the waist size and position in the near and far field. The laser beam size is controlled by adjusting the separation between the collimating lens and laser facet. Approximate collimation is achieved when the laser spot exhibits a minimum

variation in beamwidth when viewed near the laser facet and several meters away. The final collimation adjustment is performed with a collimation tester after the beam propagation direction is established.

The following procedure is performed to establish the proper beam height and align the beam propagation direction parallel to the laser baseplate. The system is designed for an optical axis 1.057 inches above the main baseplate. The proper beam height is achieved by making small adjustments in the laser diode height while monitoring the laser spot several meters away. When the laser beam is centered near 1.057 inches above the surface of the optical table, the beam height is correct. The beam height is checked at several separations from the laser to verify that the laser propagation direction is parallel to the baseplate.

The procedure for aligning the laser beam in the transverse direction is similar to the elevation alignment procedure with the exception that the laser assembly is rotated 90^{o} and is lying on its side. The lateral diode positioning screws are adjusted until beam position above the table surface is the same for observation planes near the laser facet and several meters from the laser. The laser propagation in the transverse direction is now aligned parallel to the Table surface and to the reference edge of the laser source subassembly.

Since the beam collimation is a sensitive function of the laser-lens separation, the final beam collimation adjustment is performed after the laser propagation direction is established. A beam collimation tester is utilized to determine the optimum lens position to achieve collimation. An additional collimation measurement is performed after the source assembly is completed since the expanded beam allows a more accurate determination of collimation.

With the laser properly aligned, the half-wave plate and optical interference filter can be installed to complete the laser subassembly. The polarization of the optical beam is governed by the incident polarization requirements for the Bragg cells. TeO_2 slow-shear cells require a vertical incident polarization and consequently, the laser polarization must be rotated 90^{o} using a half-wave plate. Using a detector with a vertically oriented polarizer, the half-wave plate is rotated until the maximum detector output is observed. With the source optical polarization aligned in the vertical plane, the half-wave plate is locked in position.

Optical reflections that feedback into the laser can induce fluctuations in the laser output. Components and mounts should be designed to minimize optical reflections and backscatter. Some suggestions for improving the system in this regard are presented in the Section 3.3.5.3.

Because of manufacturing problems with the optical interference filter which adversely affected the transmittance, it was necessary to fabricate a second set of filters. While the new filters were fabricated, the tests described in this report were conducted. Although the new filters have been received, they are not currently installed in the current POC configuration.

With the completion of the laser alignment, the laser subassembly is secured to the main baseplate along with the beam expansion mounting fixture. The alignment of the beam expander is relatively straightforward since reference mounting surfaces are provided for all four beam

expansion prisms. Each prism is aligned in succession, beginning with the smallest element, by making minor adjustments in their positions so that the beam is centered within their clear aperture. After all four elements have been properly aligned, they are fixed in position, completing the fabrication and alignment of the source assembly.

The optical insertion loss of the anamorphic beam expander is 1.4 dB and is determined from the ratio of the measured optical power entering and exiting the device.

The final characterization of the source assembly is performed by confirming the collimation using the collimation tester and measuring the profile of the expanded output beam using a scanning point detector. The measured output beam profile reveals a $1/e^2$ full-width of 19.7 mm which is in agreement with the requirements for the POC model.

3.2.2.2 Interferometer

A diagram of the MCDD optical processor is presented in Figure 3.1-8. The laser source assembly, consisting of the laser and beam expander subassemblies, is located in the upper right portion of the diagram. The expanded beam exiting the source assembly is directed into the narrowband interferometer with a single fold mirror.

In the interferometer, the light is divided at the beam splitter into the two arms of the interferometer. In one path, the beam passes through an expansion prism to provide a 5% increase in the beamwidth , while the beam in the other path is decreased by approximately 5% in propagating through a prism oriented for a slight beam compression. Each arm of the interferometer is folded through a Bragg cell using a mirror with tilt adjustments for precise beam alignment. The unequal beamwidths in the two branches of the interferometer are 20.7 mm and 18.7 mm in the signal and reference paths, respectively. The asymmetry of the interferometer stipulates that the RF signal must be applied to the cell in the wider beam path and the reference comb to the cell in the narrower beam path in order to optimize system performance.

The beams from the two Bragg cells are combined in the beam splitter and focused onto a common photodetector by the transform optics. When the interferometer is aligned properly, the first diffraction orders from the Bragg cells will overlap and mix to an IF of 320 MHz.

In order to properly align the interferometer mirrors, the Bragg cells are removed from the processor. Without modulation, the two optical beams homodyne, creating a static interference pattern which is determined by the relative phase difference in the beam paths. The tilt of the corner mirrors is adjusted so that the laser spot exiting the interferometer is 1.057 inches above the baseplate. While observing the interference pattern with an infrared viewer, the mirrors are adjusted until a single, uniform fringe is apparent at the output of the interferometer. The two beams are now collinear and the preliminary mirror alignment has been completed.

In the Bragg cell alignment, after inserting both cells into the interferometer, the height is adjusted to align the incident beam in the center of the acoustic aperture. While viewing the output, the roll and tilt of the cells are adjusted until a single, uniform fringe is observed. Subsequently, an

RF signal sweeping from 50 MHz to 90 MHz is applied to the transducer in one arm of the interferometer and the light in the other path is blocked with an opaque card. While viewing the scanning first diffraction order, the illuminated cell is rotated to optimize the acousto-optic response over the 40 MHz bandwidth. When the optimum uniformity across the band is observed, the Bragg condition is satisfied and the cell is secured to prevent further rotation. The swept RF signal is subsequently transferred to the cell in the other arm of the interferometer and the optimization procedure is repeated for the second transducer.

To verify the proper alignment of the Bragg cells, a 70 MHz CW signal is coupled through a two-way power divider with an output connected to each transducer. Since the RF signal modulates both paths of the interferometer, the first diffraction orders will homodyne creating a static fringe pattern. A single, uniform fringe is generated by making a slight adjustment in the roll and tilt of the cells. The Bragg cells are now properly aligned.

The final adjustment of the interferometer entails aligning the corner mirrors to optimize the overlap of the first diffraction orders for the 320 kHz intermediate frequency. A CW modulation signal of 70 MHz and 70.32 MHz is applied to the signal and reference cells, respectively. The diffracted beams are focused onto a photodetector which is coupled to an RF spectrum analyzer. Fine adjustments in the tilt of the mirrors are made while the signal power at 320 kHz is monitored on the display. When the maximum power at the IF is observed, the mirrors are properly positioned.

3.2.2.3 Transform Optics

The optical system for focusing the diffracted energy onto the photodetectors is a folded, compound lens system. The design consists of an positive achromat with a focal length of 302 mm and two closely spaced negative elements each with a focal length of -100 mm, as illustrated in Figure 3.2-6. The separation between the achromat and the first negative element, and the two negative lenses is approximately 264 mm and 4.892 mm respectively. This lens combination yields an effective focal length of 676 mm in a physical length of 287 mm.

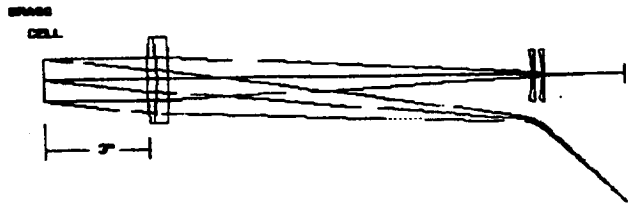

2-7-91

Figure 3.2-6 Positive Achromat Design

The beam waist measured at the focal plane of the transform optics is 39 microns. The beam profile is measured by scanning an integrated point detector and 5 micron wide slit through the focused spot. The actual laser waist formed by the transform optics is less than 39 microns since the measured beamwidth is the convolution of the actual beam profile with the 5 micron aperture function.

3.2.2.4 Photodetector

The photodetector is a Motorola MFOD 1100 PIN detector which is reversed biased with a 15 volt supply. In order to simulate a single channel in the output plane, the detector aperture is limited by an 18 micron wide slit. The detector/slit combination can be translated along the focal plane using a precision translation stage to demonstrate the parallel channelization of the POC model.

3.3 Test and Evaluation

A test plan and procedure has been developed to demonstrate the performance of the POC model. A set of STE equipment is configured to execute the tests contained in the test plan. This section describes the STE equipment configuration and details the performance evaluation tests performed on the POC model.

3.3.1 Special Test Equipment Configuration

A manually operated STE configuration was implemented for POC narrowband demultiplexer testing. This STE configuration consists entirely of off-the-shelf subsystems and components to facilitate the evaluation of demultiplexer dynamic range, bit error rate and adjacent channel rejection measurements. A high level STE block diagram is depicted in Figure 3.3-1. This configuration generates a pseudorandom (PRN) coded QPSK modulated carrier for injection into the POC signal Bragg cell. Impairments are generated including a PRN coded QPSK modulated adjacent channel carrier and Gaussian noise. Measurement equipment is included for POC performance evaluation. Each of the major STE subsystems is described in the following sections.

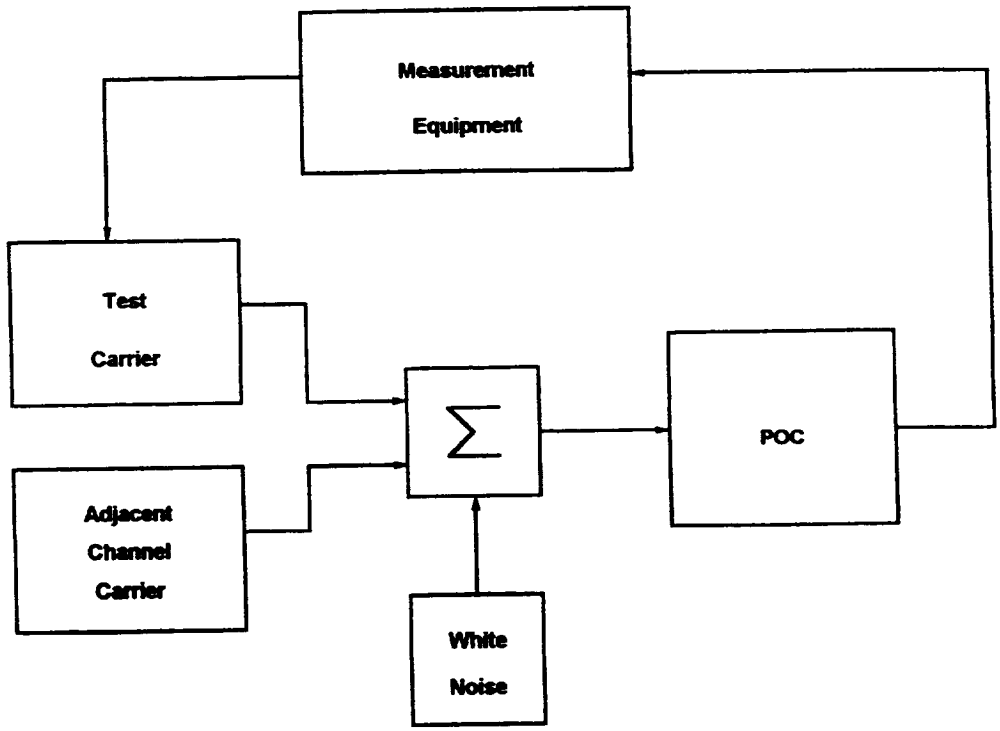

Figure 3.3-1 Top Level STE Block Diagram

3.3.1.1 Test Carrier

The test carrier to be injected into the POC demultiplexer is a PRN coded QPSK modulated signal. The PRN code is generated by a TTC Bit Error Rate Tester (BERT). The code length used by the BERT is 2^{20}-1. The BERT generates both DATA and CLOCK outputs to the modulator. The modulator is a Comstream CM421 modem which was supplied by NASA LeRC

to facilitate modulation and demodulation of the carrier. This modem requires a special interface to the BERT which supplies the modem with DATA, DATA Inverted and CLOCK. The modem modulates the carrier to an IF frequency of 70 MHz. The bandwidth of this carrier is 50 MHz. This channel width is due to the characteristics of the modem. The desired channel bandwidth is 40.0 kHz. The bit rate of the carrier is 64 kbps. The modulated carrier is filtered by the transmit filter and attenuated to the appropriate level with a 6 dB pad. The transmit filter is a six-pole Butterworth filter as described in Section 3.1.1.6. The filtered carrier is fed to the IF input port of the HP Noise and Interference Test Set as described in Section 3.3.1.3.

3.3.1.2 Adjacent Channel Carrier

The adjacent channel carrier is generated to serve as a source of adjacent channel interference. The adjacent channel carrier is implemented as a PRN coded 32 kbps BPSK modulated carrier. This implementation is spectrally equivalent to a 64 kbps QPSK carrier. It was selected for ease of implementation. The PRN coded signal is mixed with a CW carrier at 70.04 MHz generated by an HP Vector Signal Generator. The modulated carrier output from the mixer is filtered by a transmit filter and brought to the appropriate level through an attenuator/amplifier pair. The filter characteristic of this transmit filter is identical to the test carrier transmit filter with a center frequency of 70.04 MHz. The adjacent channel carrier is fed into the Interference Input port of the HP Noise and Interference Test Set.

3.3.1.3 POC Signal Channel

The HP Noise and Interference Test Set has the capability to accept a Test Carrier (C) and an Interference Carrier (I). The test set has an internal noise generator which can be controlled to vary the desired E_b/N_0 at the demodulator. The composite carrier, interference and noise is available at the HP Noise and Interference Test Set IF Output port. This output signal is amplified and fed as input to the POC signal Bragg cell.

3.3.1.4 Reference Comb Generator

In order to perform heterodyne detection to a common IF in the POC demultiplexer, the reference signal must be a frequency comb, with frequency spacing equal to that of the desired channel spacing and bandwidth greater than or equal to the overall system bandwidth. The MCDD system requires two reference combs, one for the narrowband and wideband systems respectively. These are generated using repeating PRN sequences, an approach requiring minimum power among several alternatives. In order to begin with a relatively flat spectrum across the bandwidth of the POC, the bandwidth of the main lobe of the sinc-function shaped PRN spectrum was selected to be four times the MCDD bandwidth. In this way, the central 25% of the spectrum is selected by bandpass filtering which further flattens the desired band. The narrowband and wideband PRN sequence generators are shown in Figures 3.3-2 and 3.3-3 respectively.

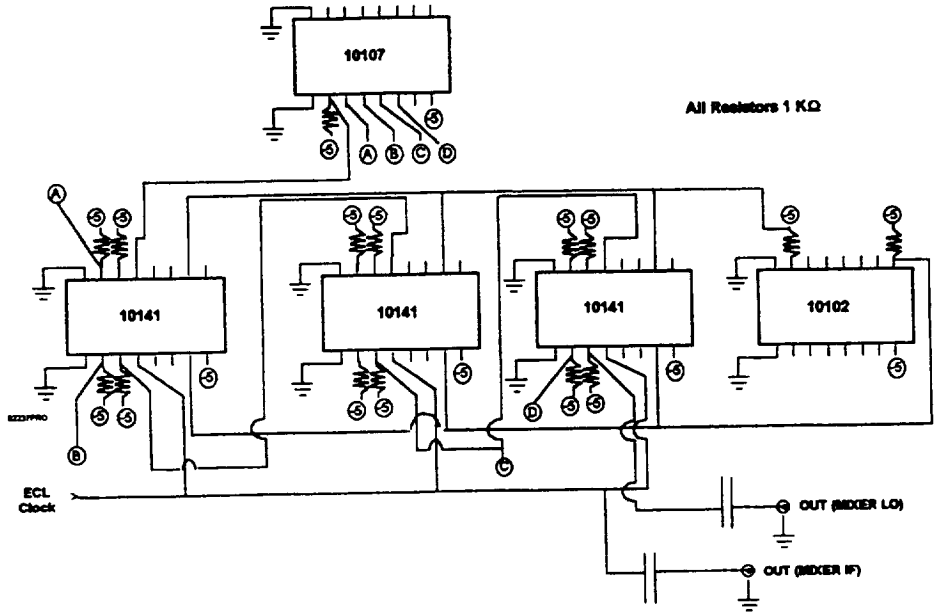

Figure 3.3-2 Repeating PRN Sequence Generator - Narrowband Processor

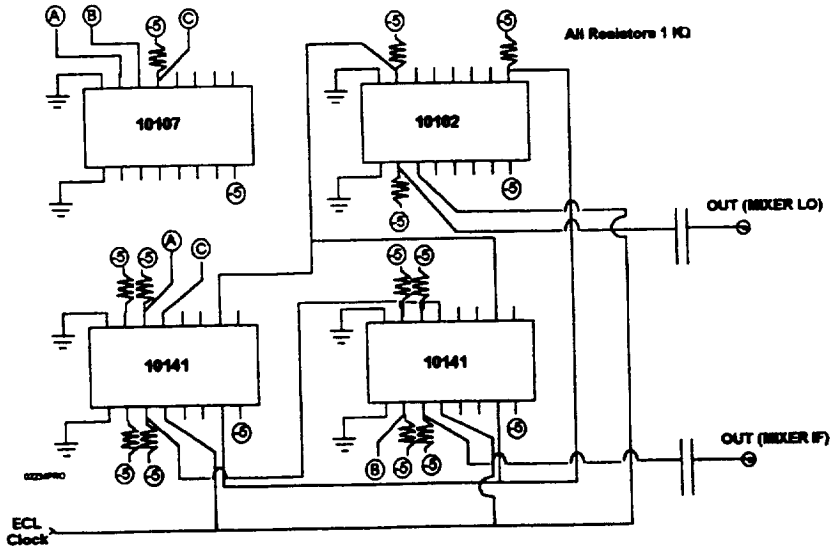

Figure 3.3-3 Repeating PRN Sequence Generator - Wideband Processor

The Reference Comb Generator is shown in Figure 3.3-4. For the narrowband system accommodating 1000 channels, an 11-stage shift register sequence generator is used to generate a 2047 length sequence. For a clock frequency of 80 MHz, the sequence repeats every 25 msec providing comb lines every 40 kHz. Main lobe bandwidth is 160 MHz, providing reasonable flatness over 40 MHz. A two-stage bandpass filter was designed with a "dip" in the middle of its frequency response to further flatten the spectrum. Similarly, the wideband system comb generator, requiring only 40 comb lines, uses a 7-stage shift register sequence generator which generates a 127 length sequence. For a channel spacing of 960 kHz, the sequence is required to repeat every

1.04 MHz. Thus, a clock frequency of 122 MHz is used, and the main lobe of the PRN spectrum covers 244 MHz. The 40 MHz MCDD bandwidth is, therefore, less than 20% of the main lobe, with even greater flatness than the narrowband comb generator.

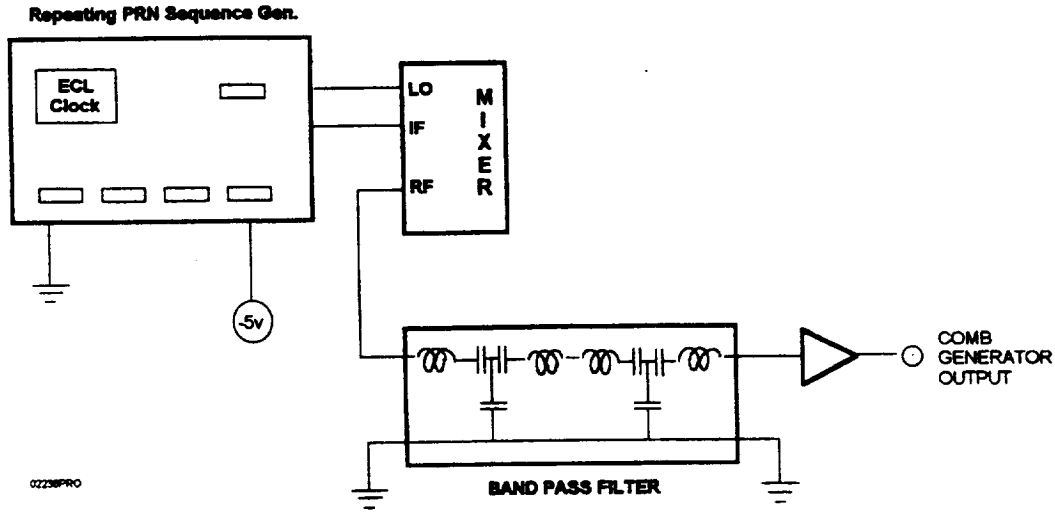

Figure 3.3-4 Reference Comb Generator

Both comb generators were fabricated and tested, verifying the predicted performance. Since the wideband optical system was not fabricated, only the narrowband comb generator was tested in actual system operation.

3.3.1.5 MCDD Detectors and Test Detection Circuitry

The optical detectors and detection circuitry for the POC demultiplexer need not accommodate the RF signals being analyzed, but must be appropriate for the chosen common IF, the offset between reference comb line and signal frequency which will overlay it. In this case, although potential carriers fall between 50 MHz and 90 MHz, the detector IF is 320 kHz with a channel bandwidth of 40 kHz, so that the maximum frequency to be processed at any detector is less than 400 kHz. Whether the processing is being performed by a test detector and its related circuitry or by a detector array with integrated processing circuitry, the heterodyne detection is performed in two stages: (1) optical heterodyne detection between a signal and reference producing output at the difference frequency (here 320 KHz with a bandwidth of 40 kHz) and (2) demodulation of the QPSK data.

The detector circuitry is shown in Figure 3.3-5. The photodetector implemented in the POC is a Motorola MFOD 1100. This detector is AC coupled (with a DC blocking capacitor) to an Analog Devices AD509 operational amplifier. Since the relatively large-area photodetector (compared to the pixel size of one channel) would include many channels, an area-limiting slit is used to reduce the acceptance area of

the detector. Finally, a bandpass filter is used to remove extraneous signals; however, the passband of this filter is large compared to the input filter of the demodulator so that it does not affect the channel characteristics of the MCDD. Since the demodulator contains an input filter, the main purpose served by the post-detector filter is to provide a cleaner signal to the oscilloscope used to view the detected signal during alignment of the detector.

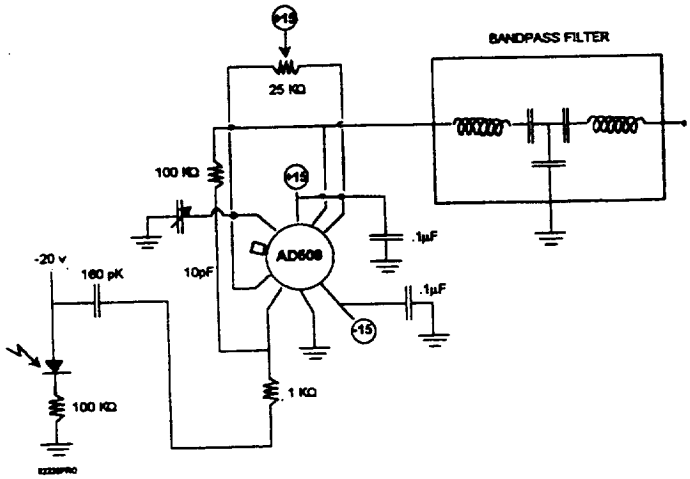

Figure 3.3-5 Photodetector and 320 kHz IF Amplifier

3.3.1.6 Demodulation and Measurement

The 320 kHz output signal from the POC detection circuitry bandpass filter is amplified and mixed with a CW signal from a signal generator at a frequency of 70.320 MHz. This frequency is used to upconvert the POC output signal to a 70.0 MHz IF. The 70.0 MHz IF signal is fed into the Comstream modem Receive IF port for demodulation. The demodulated data is directed to the oscilloscope for data monitoring of the PRN code. The data is also provided as input to the BERT Receive DATA port for bit error rate evaluation. The test carrier originally generated by the BERT has been modulated, combined with interference and noise, demultiplexed by the MCDD POC, optically detected, demodulated and returned to the BERT for error rate analysis.

3.3.2 Measurement Configurations and Test Procedures

This section describes the plans and procedures for testing the narrowband POC model. These tests are a subset of the original MCDD test plan which fully characterizes the narrowband and wideband demultiplexers.

The conducted tests are listed below.

1. Single Channel Dynamic Range
2. Single Channel Dynamic Range with Adjacent Channel Loading
3. Single Channel Dynamic Range with Multiple Channel Loading
4. Adjacent Channel Rejection
5. Modem-Only Single Channel BER vs Eb/No

6. Single Channel BER vs Eb/No
7. Single Channel BER vs Eb/No with Adjacent Channel Loading

3.3.2.1 Single Channel Dynamic Range

This test examines the linear operating region of an individual narrowband carrier through the POC demultiplexer. A CW carrier is stepped in power from the system noise floor to system saturation.

The test setup is depicted in Figure 3.3-6. An unmodulated CW signal is generated by the HP Vector Signal Generator as input to the signal Bragg cell of the POC model. The frequency of the CW signal is 70.0 MHz. The level of this signal is varied in 2 dB steps and the resulting output power is measured by the spectrum analyzer.

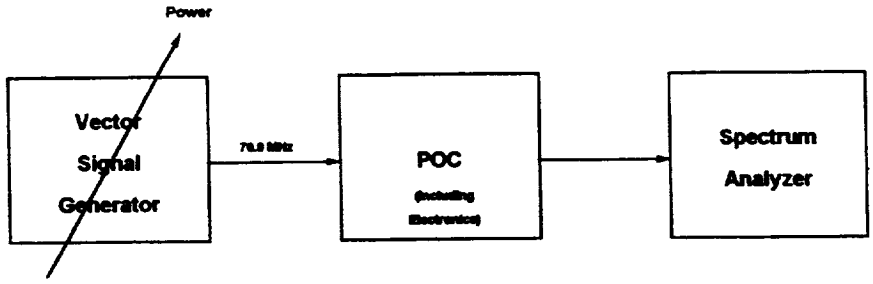

Figure 3.3-6 Single Channel Dynamic Range Setup

A plot is generated indicating input power vs output power through the POC. This plot provides an indication of the linear operating region of the POC.

3.3.2.2 Single Channel Dynamic Range with Adjacent Channel Loading

This test is similar to the Single Channel Dynamic Range test. In addition to the CW carrier at 70.0 MHz, a CW adjacent channel carrier is introduced at 70.04 MHz. The nominal power of the adjacent channel is 0 dBm. This level is 30 dB below the composite power level at which the POC is 100% diffraction efficient. In order to potentially accommodate 1000 narrowband channels, the nominal operating level of an individual channel is set to 0.0 dBm.

The test setup is depicted in Figure 3.3-7. An additional signal generator is included to generate the adjacent carrier. This signal generator is set to a frequency of 70.04 MHz and a level of 0.0 dBm. As above, the level of the inband test signal is varied in 2.0 dB steps and the resulting output power is measured by the spectrum analyzer.

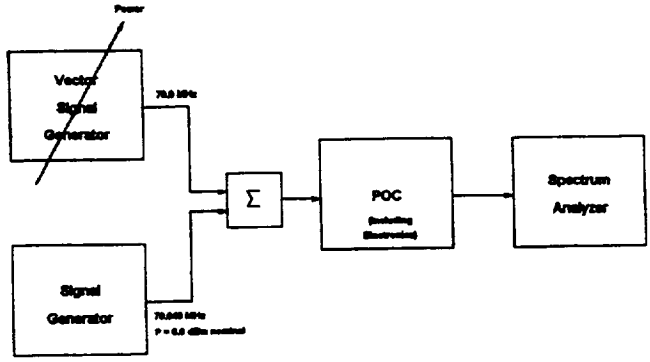

Figure 3.3-7 Single Channel Dynamic Range With Adjacent Channel Loading

A plot is generated indicating input power vs output power through the POC. This plot provides a comparison to the measurements in the Single Channel Dynamic Range test. Any changes in the linear operating region of the POC due to the presence of the adjacent channel are noted.

3.3.2.3 Single Channel Dynamic Range with Multiple Channel Loading

This test is similar to the Single Channel Dynamic Range test. In addition to the CW carrier at 70.0 MHz, multiple CW loading carriers are generated in the MCDD 40 MHz bandwidth. The STE generates the carriers spaced 1 MHz apart. The nominal composite power of the loading carriers is +14 dBm. This level is selected to give the 40 loading carriers the equivalent level of 1000 carriers each at a level equal to the test signal (0 dBm).

The test setup is depicted in Figure 3.3-8. The wideband reference comb generates carriers at baseband. This comb is mixed to a center frequency in the vicinity of 70.0 MHz such that none of the loading carriers fall within the test band of 70.0 MHz +/- 40 kHz. An amplifier after the mixer brings the level of the composite loading carriers to +14 dBm. As above, the level of the inband test signal is varied in 2 dB steps and the resulting output power is measured by the spectrum analyzer.

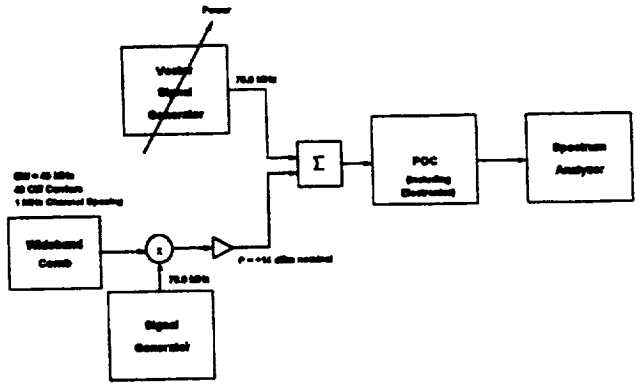

Figure 3.3-8 Single Channel Dynamic Range with Multiple Channel Loading

A plot is generated indicating input power vs output power through the POC. This plot

provides a comparison to the measurements in the previous dynamic range tests. Any change in the linear operating region due to multiple channel loading is noted.

3.3.2.4 Adjacent Channel Rejection

This test demonstrates the POC's in-band rejection of adjacent channel interference. An unmodulated CW adjacent channel carrier is stepped in frequency from the center of the test channel (70.0 MHz) to the far edges of the adjacent channels (69.94 MHz and 70.06 MHz). The frequency is stepped in 2 kHz increments. A spectrum analyzer at the output of the POC is used to measure the resulting power inband at each frequency step of the adjacent carrier.

The test setup is depicted in Figure 3.3-9. A Vector Signal Generator is used to provide the CW carrier at a nominal level of 0 dBm as discussed above. This carrier is input to the POC signal Bragg cell. The spectrum analyzer measures the resultant power inband.

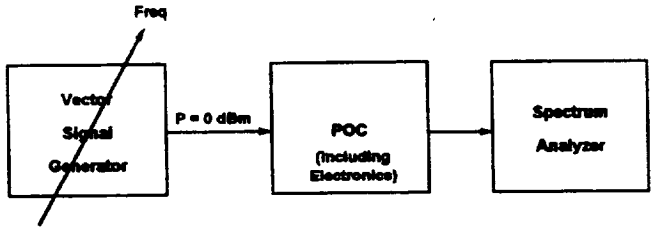

Figure 3.3-9 Adjacent Channel Rejection

A plot is generated indicating inband power vs adjacent channel frequency offset. This plot provides an indication of the power measured inband due to the adjacent carrier. This provides a measure of the POC's adjacent channel rejection capability.

3.3.2.5 Modem-Only Single Channel BER vs Eb/No

The Comstream modem implemented in the STE is not correctly matched to the POC demultiplexer's filter characteristic. The modem uses 50 kHz channel spacing while the POC is designed to accommodate 40 kHz channels. In addition, the transmit and receive filters of the modem have unknown characteristics. Therefore, prior to testing the BER of the optical demultiplexer, a series of tests are run without the POC. These tests provide a reference characterization of the test configuration. The POC is then inserted and further BER tests are conducted. A comparison between the two tests facilitates a determination of the performance degradation due to the POC.

The initial modem-only configuration is shown in Figure 3.3-10. The BERT is setup to generate a PRN code which is input to the modulator section of the Comstream modem via special interface electronics required by the modem. The modem modulates the carrier to a frequency of 70 MHz. The modulated signal is input to the HP Noise and Interference Test Set. This unit combines the input signal with adjustable Gaussian noise to set the desired E_b/N_0. The carrier and noise are fed back to the demodulator section of the modem. The demodulated carrier is returned to the BERT for error rate evaluation.

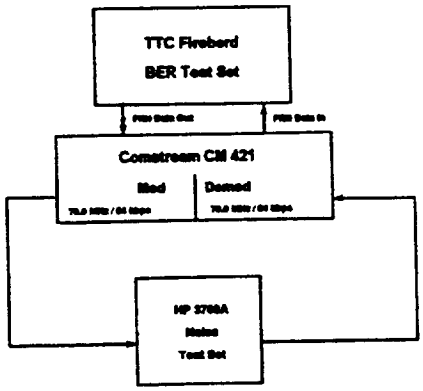

Figure 3.3-10 Modem-Only BER Setup 1

A plot is generated of Bit Error Rate vs Eb/No for the range of BER from 10^{-2} to 10^{-7}. This plot indicates the BER performance of the modem in the MCDD STE configuration. This is used as a reference for subsequent measurements.

After the above BER curve has been generated, an attenuator and 70.0 MHz channel filter are included in the transmit/receive chain. This test configuration is shown in Figure 3.3-11. The attenuator is used to simulate the approximate insertion loss of the POC demultiplexer. The channel filter simulates the filter characteristic of the POC model for a 40 kHz wide channel.

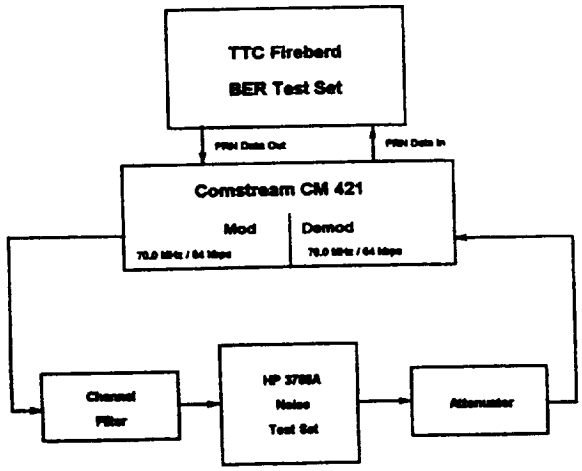

Figure 3.3-11 Modem-Only BER Setup 2

The above test is run again to generate a second BER vs Eb/No curve. This curve indicates the effect of having two receive filters in the system: the MCDD POC and the modem 50 kHz filter. This measurement more accurately simulates the POC/STE configuration to be subsequently tested. Again, these two curves do not provide performance measurements of the POC, but rather a measurement reference.

3.3.2.6 Single Channel BER vs Eb/No

This test characterizes the BER vs Eb/No performance of a modulated PRN signal at 70.0 MHz. The procedures and setup for this test are identical to those in the "Modem-Only Single Channel BER vs Eb/No" test with one exception. The POC demultiplexer and associated electronics are now in the signal path. In this test no other interferers are present. The inband test carrier is combined with noise at the HP Noise and Interference Test Set to establish the desired E_b/N_0.

The test configuration is shown in Figure 3.3-12. The BERT is setup to generate a PRN code which is input to the modulator section of the Comstream modem. The modem modulates the carrier to a frequency of 70.0 MHz. The modulated signal is input to the HP Noise and Interference Test Set. The signal and noise are input to the POC signal Bragg cell and through the 70.0 MHz transmit filter. The filtered channel is fed back to the demodulator section of the modem. The signal is demodulated and returned to the BERT for error rate measurements.

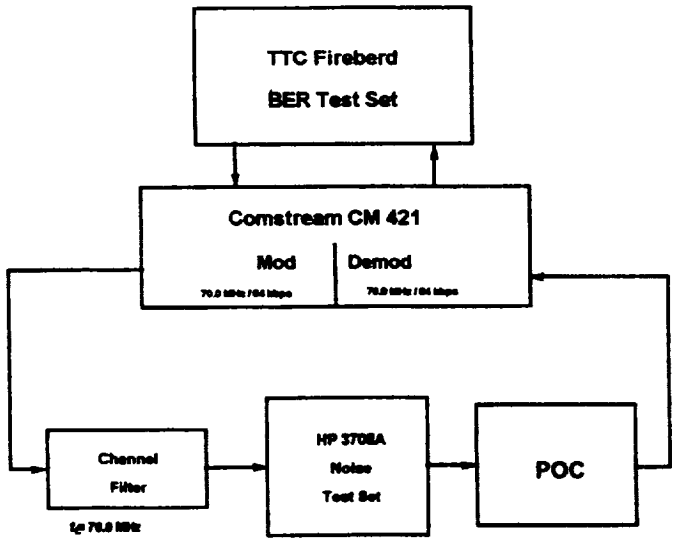

Figure 3.3-12 Single Channel BER Setup

A plot is generated of bit error rate vs Eb/No for the range of BER from 10^{-2} to 10^{-7}. This plot indicates the BER performance of the POC demultiplexer. Comparison of this data with the Modem-only BER plot provides an indication of the performance degradation associated with the POC.

3.3.2.7 Single Channel BER vs Eb/No with Adjacent Channel Loading

This test characterizes the BER vs E_b/N_0 of a modulated PRN signal at 70.0 MHz in the presence of a modulated PRN adjacent channel carrier at 70.04 MHz. The procedures and setup for this test are identical to those in the Modem-Only Single Channel BER vs Eb/No with Adjacent Channel Loading test with one exception. The POC demultiplexer and associated electronics are now in the signal path. The inband and adjacent channel carriers are combined with noise at the HP Noise and Interference Test Set.

The configuration for this test is shown in Figure 3.3-13. A 32 kbps PRN sequence generator is mixed with a 70.04 MHz carrier from the Vector Signal Generator. The modulated carrier is passed through a transmit filter which has a center frequency of 70.04 MHz. The resultant signal is combined with the filtered modulated test carrier and noise at the HP Noise and Interference Test Set. The test and adjacent channel carriers and the noise are input to the POC signal Bragg cell. The demultiplexed carrier is fed back to the demodulator section of the modem. The signal is demodulated and returned to the BERT for error rate evaluation.

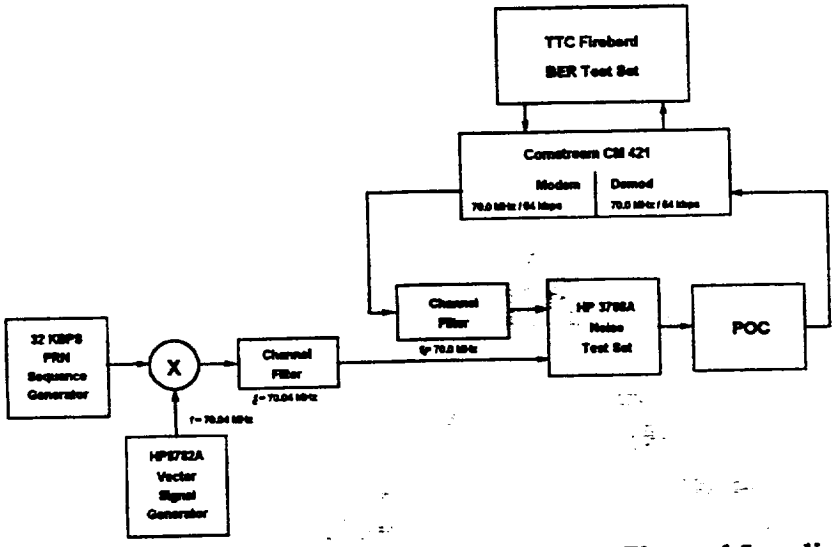

Figure 3.3-13 Single Channel BER With Adjacent Channel Loading Setup

Two plots are generated of BER vs E_b/N_0 for BER in the range of 10^{-2} to 10^{-7}. The first set of BER measurements are taken with the inband signal and adjacent signals of equal levels. In the second set of measurements the inband carrier level is kept 8.0 dB below the level of the adjacent channel to evaluate faded channel performance. Both plots indicates the BER performance of the POC demultiplexer in the presence of a modulated adjacent channel. Comparison of this data with the Modem-Only BER plot provides an indication of the performance degradation associated with the POC.

3.3.3 POC Test Results

The POC consists of the optical baseplate, the comb generator and power amplifiers that feed the reference Bragg cell, the detector amplifier and bandpass prefilter and a local oscillator, mixer and output amplifier to shift the IF signal onto a 70 MHz carrier.

The characterization of the processor consists of three fundamental measurements: dynamic range, adjacent channel rejection, and bit-error rate (BER). These measurements are performed under test conditions described in Section 3.3.2. The dynamic range and adjacent channel tests are measurements which utilize unmodulated carriers as test signals. The bit-error rate measurements employ phase-shift keyed modulated carriers for test and evaluation.

3.3.3.1 Dynamic Range Measurements

The dynamic range measurements reveal the operating range over which the input and output are linearly related for a channel in the demultiplexer. In the single channel dynamic range measurement (Figure 3.3-6) a 70 MHz CW signal from a Vector Signal Generator is coupled through an amplifier into the POC. As the power at the input to the demultiplexer is varied, the output power at the 70 MHz output carrier frequency is measured on a spectrum analyzer. To simulate the receiver channel, the resolution bandwidth on the spectrum analyzer is set to 30 kHz. A plot of measured output power as a function of the input signal level, depicted in Figure 3.3-14, demonstrates a linear dynamic range of nearly 50 dB. The nonlinear response near the maximum power level is attributed to the input amplifier which exhibits a 1 dB compression point near +15 dBm. Consequently, a 50 dB linear dynamic range is measured for a single channel of the POC and is limited by the nonlinear response of the input amplifier.

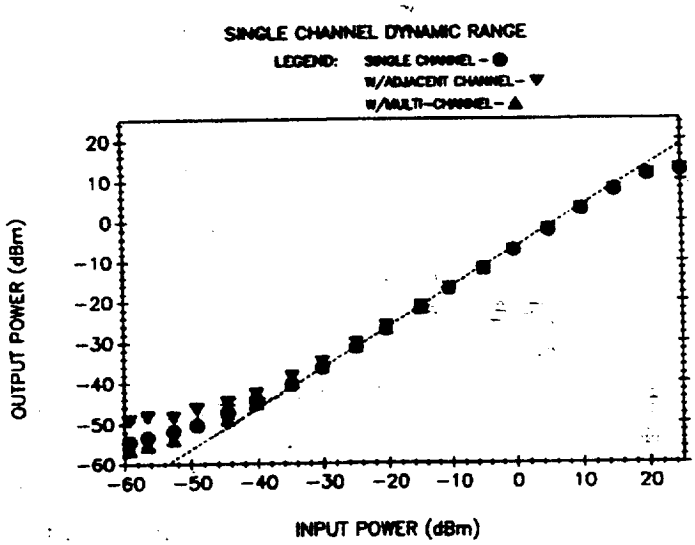

Figure 3.3-14 POC Single Channel Dynamic Range

To determine the linear operating range in the presence of an adjacent channel signal, a second CW signal at 70.04 MHz is summed with the test carrier and applied to the input of the signal Bragg cell. During the measurements, the adjacent channel signal power is maintained at 0.0 dBm while the test carrier power is varied from the noise floor to near saturation. A plot of the input vs output power for the 70 MHz carrier is displayed in Figure 3.3-14 in the presence of the adjacent channel signal and reveals a decrease in the linear dynamic range to approximately 40 dB.

The final dynamic range measurement is performed with multiple channel loading. The multiple carriers are generated using the wideband comb circuit which provides forty unmodulated carriers at baseband with a frequency spacing 1 MHz. The frequency comb is translated into the POC band by mixing the comb with a local oscillator. The total power in the out-of-channel signals is

+24 dBm and was amplifier limited. The signal channel measurements are performed at 70.0 MHz. The out-of-channel signal closest to the measurement frequency is separated by 200 kHz at 70.2 MHz. The results of the multi-channel loading are nearly identical to the original single channel measurements, yielding approximately 50 dB of linear dynamic range. A comparison of all three dynamic range measurements is presented in Figure 3.3-14.

3.3.3.2 Adjacent Channel Rejection

In order to determine the POC filter response and the extent to which adjacent channel interference is rejected, a CW carrier is sequentially stepped from the channel center frequency to the far edge of the adjacent channel while the power in the signal band is measured. The input to the POC is a CW carrier at a nominal power level of 0.0 dBm. As the input frequency is stepped through the signal and adjacent channel, the output power at the channel center frequency is monitored on a spectrum analyzer. The plot of the signal power as a function of the offset from the channel center frequency is presented in Figure 3.3-15. In these measurements, the resolution bandwidth of the spectrum analyzer is 30 kHz to closely approximate the channel bandwidth.

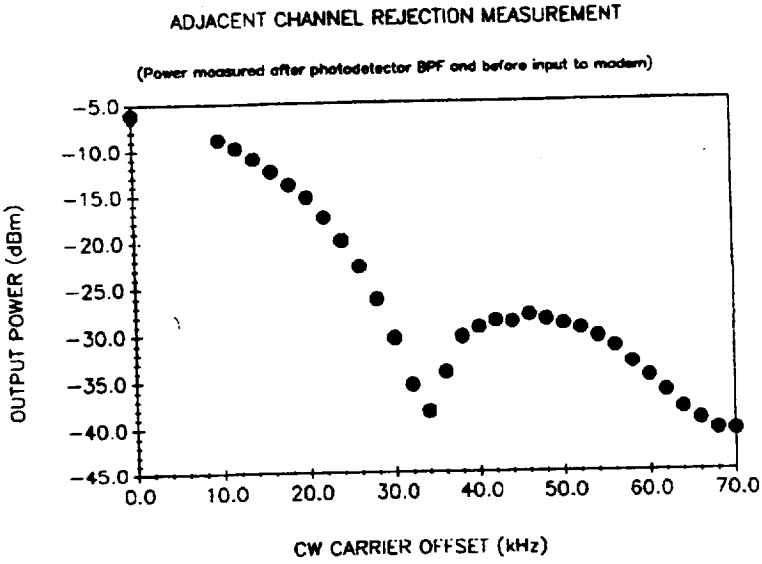

Figure 3.3-15 Adjacent Channel Rejection

3.3.3.2 Bit Error Rate

In order to evaluate the bit error rate (BER) of the POC, three pieces of test equipment are necessary: the BER test set (BERT), the modem, and the noise test set. In all of the measurements in this section, these three components are configured as presented in Figure 3.3-10.

The BERT performs several critical functions including the generation of a pseudo-random code sequence used to modulate the transmit carrier and the determination of the BER based upon a comparison of the transmitted and received data sequences. The BER for a given set of test

conditions is displayed on the front panel and can be dumped to a printer through the RS-232 serial port. This is an extremely useful feature since some of the lower BER measurements require excessive measurement times. To ensure that the BER measurements are accurate, in the "auto mode", the error rates are not determined until more than one hundred errors have accumulated.

The pseudo-random sequence generated by the BERT is fed to the modem which utilizes the input sequence to QPSK modulate the transmit carrier. The modulated signal is coupled into the RF port of the Noise Test Set which monitors the input power level and combines the signal with the appropriate noise level. The noise density generated in the test set is determined based upon the level required to establish the E_b/N_0 entered from the front panel of the equipment.

The signal plus noise is connected to the receiver portion of the modem which demodulates the QPSK signal and feeds the recovered data sequence to the BERT. The receive and transmit data are compared in the BERT and the data error rate is determined.

Since the modem utilized in these measurements has internal transmit and receive filters which cannot be disabled, the system filter response used in the measurements will be slightly different from the ideal filters in the theoretical model. Attempts to obtain the modem transmit and receive filter shapes from the manufacturer, Comstream, were unsuccessful due to the proprietary nature of the information. However, since the modem is designed for channel separations of 50 kHz, the impact upon the total filter response is expected to be minimal.

To establish a baseline for subsequent measurements, the first BER measurement is performed with only the modem, as in Figure 3.3-10. These results establish the performance limits of the test equipment and can be used as a baseline for evaluating subsequent measurements. The measured BER as a function of Eb/No is displayed as the open circles in Figure 3.3-16. The solid curve in this figure represents the ideal theoretical BER curve which does not include ISI or ACI. The modem-only BER performance is degraded by 1 to 2 dB relative to this ideal curve.

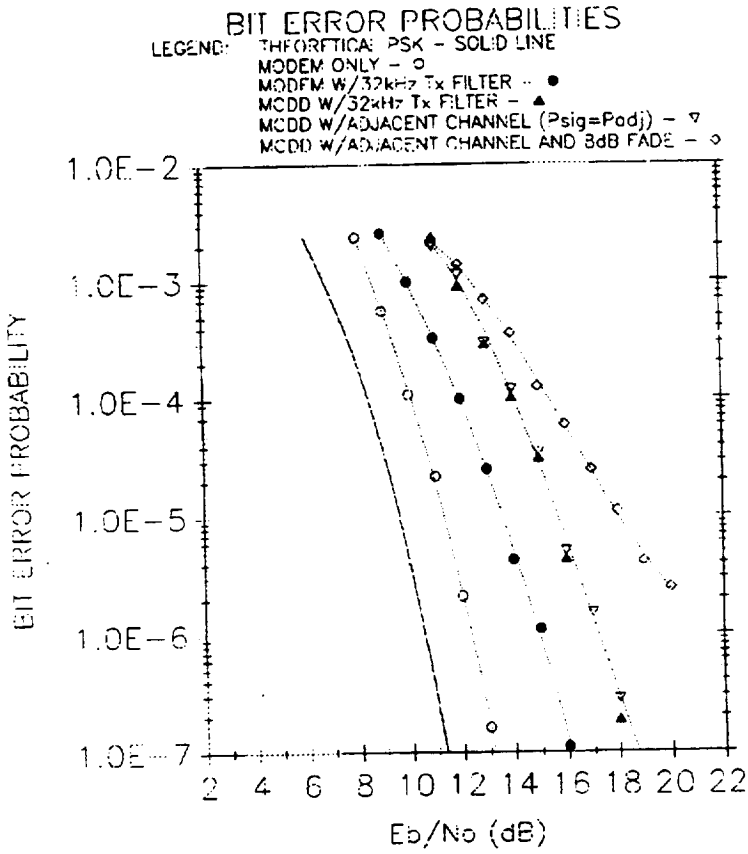

Figure 3.3-16 POC Bit Error Rate Measurements

With 64 kbps QPSK data and a transmit filter which limits the bandwidth to 32 kHz, some performance degradation should be apparent due to ISI. To evaluate the performance of the test equipment with the bandwidth limitation, the 32 kHz transmit filter is inserted in the signal path at the output of the modem, as depicted in Figure 3.3-11. The BER curve for the modem with the transmit filter is displayed as the solid circles in Figure 3.3.16 and reveals a further degradation of between 2 to 4 dB relative to the modem-only measurement.

Now that a performance baseline has been established for the test equipment, the POC is inserted in the transmit/receive path after the noise test set, as displayed in Figure 3.3-12. The output from the POC is demodulated in the receiver portion of the modem and the recovered data sequence is evaluated in the BERT to determine the BER. The transmit power level out of the modem is adjusted so that the nominal channel input power at the POC is 0.0 dBm. With a 70 MHz carrier modulated with 64 kbps QPSK, the measured BER curve is annotated with the solid triangles depicted in Figure 3.3-16. The POC exhibits a 1 to 2 dB degradation in performance relative to the modem with transmit filter BER curve. The slight increase in BER for a given E_b/N_0 is consistent since the POC provides further bandwidth reduction in the transmit/receive path.

In this test configuration, there are four filters in the signal path: the modem transmit filter, the 32 kHz channel filter at 70.0 MHz, the POC and the modem receive filter. In the system design, the

6-pole Butterworth transmit filter and the POC filter characteristics have been included as part of the design optimization. The modem filters have not been considered in the design. This point is discussed in Section 3.3.3 in which the measured results are compared with the theoretical performance.

The other critical performance characteristic is the BER in the presence of an adjacent channel signal. The modulation signal used for the adjacent channel is a 32 kbps BPSK signal which exhibits the same power spectrum as the 64 kbps QPSK channel. The test configuration for the adjacent channel BER measurement is illustrated in Figure 3.3-13. The measured spectrum of the 70.0 MHz, 64 kbps QPSK signal out of the modem is displayed in Figure 3.3-17. With each frequency division corresponding to 20 kHz (Span = 200 kHz), the significant energy outside of the 40 kHz channel bandwidth is very apparent. After passing through the 32 kHz transmit filter, the energy is concentrated within the channel bandwidth, as shown in Figure 3.3-18.

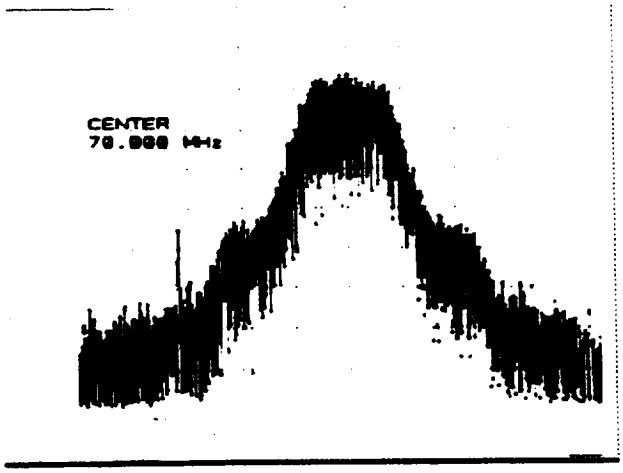

Figure 3.3-17 MCDD Comstream Modem Output - 64 kbps QPSK

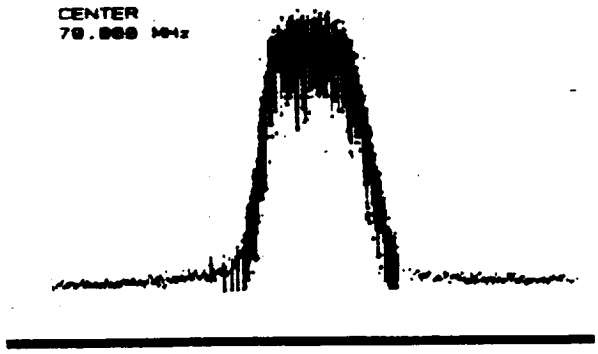

Figure 3.3-18 32 kHz Filtered Modem Output - 64 kbps QPSK

Similarly, the spectrum of the 32 kbps BPSK signal, after band-limiting by the adjacent channel filter, is displayed in Figure 3.3-19. The adjacent channel signal is coupled into the interferer port on the noise test set which is summed with the signal and noise. The spectrum of the signal and

adjacent channel is presented in Figure 3.3-20 for the case where the power in the two channels are equal. The measured BER vs E_b/N_0 for this condition is presented in Figure 3.3-16 where the data is annotated with an open triangle. The presence of an adjacent channel of equal power has a negligible effect upon the BER when compared to the single-channel-only performance.

Figure 3.3-19 MCDD Adjacent Channel - 32 kbps BPSK

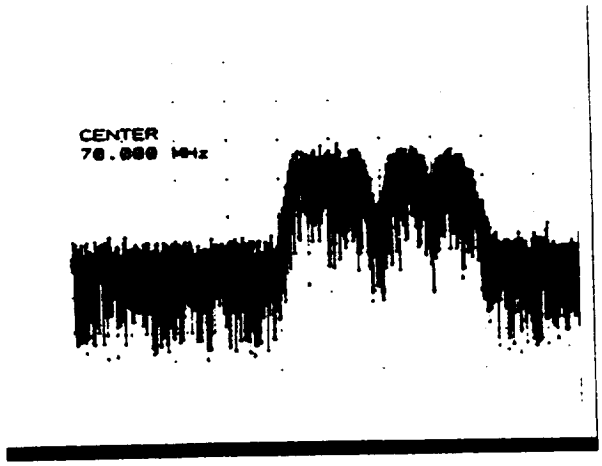

Figure 3.3-20 MCDD Test and Adjacent Channels

When the adjacent channel BER measurement is repeated with an 8 dB fade in the signal channel, a degradation of several dB is observed relative to the unfaded condition. The results of this measurement are displayed in Figure 3.3-16 with open diamonds representing the data.

3.3.4 Test Result Analysis

The analysis entails a comparison of the theoretical and experimental BER curves. The theoretical POC BER curves are plotted in Figure 3.1-7 for the performance parameters listed in Table 3.1-1. In Figure 3.3-21, the measured data, with and without an 8 dB fade, is superimposed onto the theoretical curves from Figure 3.1-7. The measured data with an 8 dB fade should be compared with theoretical Curve C.

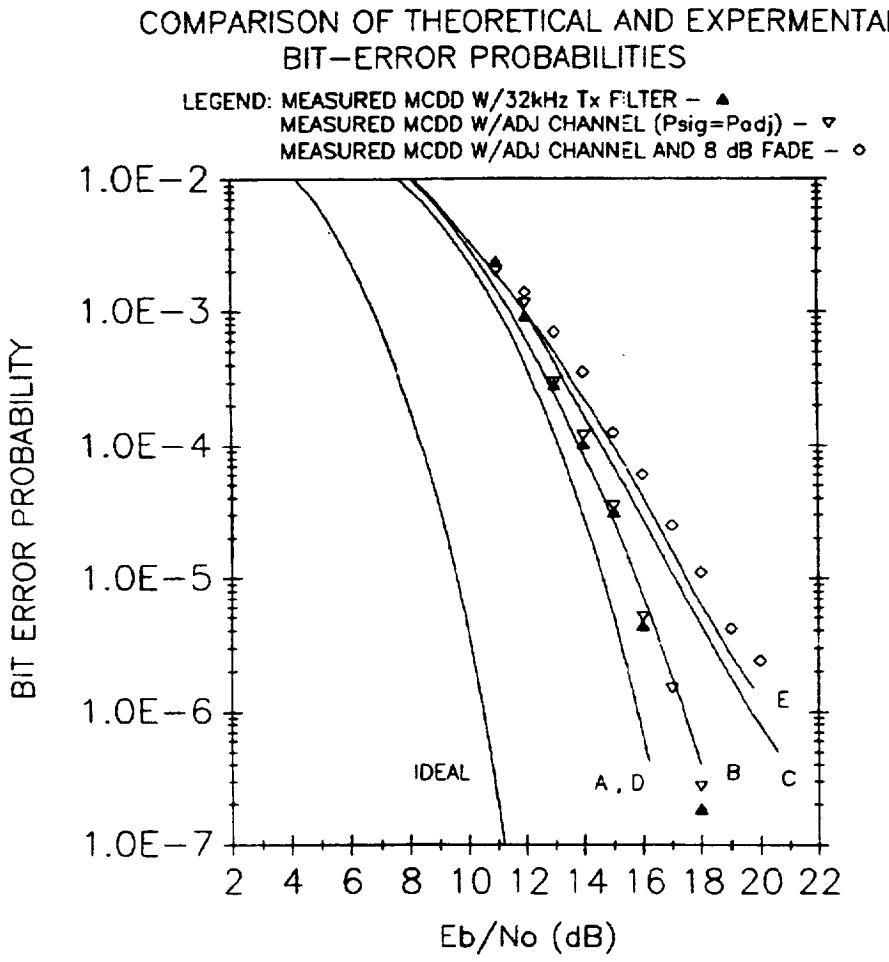

Figure 3.3-21 Measured and Theoretical BER vs. Eb/No Curves

Based upon the measured beam width of 19.7 mm at the output of the anamorphic beam expanders, the 5 % expansion and compression in the interferometer should yield signal and reference beams of 20.7 mm and 18.8 mm, respectively. These values most closely match the parameters for curve C of Figure 3.1-7 which corresponds to the BER results with an 8 dB signal fade condition. The measured performance is within approximately 1 dB of the theoretical curve C. The slightly higher bit error rate in the measured data is also consistent with additional bandwidth effects introduced by the modem transmit and receive filters which were not considered in the theoretical model.

3.3.5 Recommendations

This section provides recommendations for the optimization of future MCDD developments. These recommendations are based on observations and discussions during the design, development, fabrication and test of the MCDD POC model.

3.3.5.1 System Recommendations

This preliminary model of an Optical MCDD has shown that acousto-optic heterodyne detection RF spectrum analysis may be used for demultiplexing of FDM communications signals. The performance of this MCDD compared favorably with the performance predictions. In comparing this performance with the required system performance, a deficiency may be found. This deficiency appears to be a result of non-optimal choice of MCDD system filter characteristics. By tailoring the acoustic/optical aperture of the reference and signal paths, the filter characteristics of the optical portion of the MCDD may be modified. This filter characteristic, coupled with the transmit filter characteristic and any other receiver filter characteristic (such as that involved in the demodulation process) strongly affect system performance. However, the system design of the POC centered around a demultiplexer characterization which allows communications with inexpensive, low complexity earth stations. As such the design implements a POC transfer function which is matched to readily available ground station transmit filters. While this approach demonstrates the demultiplexing concept, optimization of the matched transmit/receive filters is recommended in order to improve the bit error rate performance of the link. Such filter optimization can be realized through pulse shaping techniques on the transmit and receive filters to eliminate ACI and ISI. First, the transmitter filters must be closely matched to the MCDD transfer function. Second, the composite transmitter filter/MCDD transfer function must approximate a Nyquist response with roll-off sufficient to minimize ACI. This design improvement should be considered in further MCDD development even though it will increase earth station cost. A system trade-off analysis between system complexity and error performance should be conducted for future MCDD demultiplexer designs.

The STE implemented the use of a government furnished modem which was not designed for a 40 kHz signal channel. The transmit and receive filter shapes of this modem are not available from the manufacturer. This hampered a through analysis of the resultant performance data. It is recommended that an appropriately matched demodulator be used in future testing of the POC to more accurately characterize system performance.

3.3.5.2 Mechanical Recommendations

The mechanical design utilized aluminum for a majority of the POC mounts. Aluminum is suitable for most of the system because of its low cost and density, and the benign environment expected within the laboratory. For future MCDD systems, however, other materials should be considered, such as composites, for lower weight, greater stability, and lower CTE. The interferometer base can be constructed of more optimal materials such as metal matrix composites which combine low CTEs and high thermal conductivity in a machinable form. These composites also offer the advantage of relatively low densities and high strength and moduli.

3.3.5.3 Optical Recommendations

An area for improvement in the Optical MCDD can be found in the choice of laser diode. The specific Mitsubishi laser which was initially sought based upon previous experience was no longer available. The "direct replacement" laser did not exhibit the same thermal stability and was not stabily "tunable" in wavelength by temperature as the previous model. Other laser diodes are now

available which exhibit the required tunability and stability. Future MCDD designs should take advantage of these laser diodes.

During the initial alignment and characterization of the POC demultiplexer, the laser output power decreased substantially over a short period of time. Further investigation indicated that the most probable cause of the laser deterioration is junction damage caused by electrical transients introduced through ground connections.

In order to eliminate the threat of device failure, the laser can is isolated from the optical baseplate and all earth ground connections. This is accomplished by securing the laser onto the thermoelectric cooler and laser mounting plate using non-conducting teflon screws.

In order to mitigate the risk of damaging the only remaining MCDD laser diode with an emission wavelength compatible with the optical interference filter, another laser with an arbitrary wavelength was mounted and aligned in the processor. This device has been operating successfully over the past 15 months without failure, confirming the diagnosis and corrective action.

In the source assembly, all planar surfaces, such as the half-wave plate, should be designed for a significant angle of incidence to minimize the potential for reflections which can feedback into the laser cavity and create modal instabilities.

In order for the POC to reliably perform channelization, the laser emission wavelength must be must be maintained within a small tolerance. The recommended approach requires the selection of a diode laser with stable longitudinal mode and a large temperature tuning range. The Spectra Diode Laboratory SDL-5412 is an example of such a device which maintains the same longitudinal mode over a range on nearly 20 degrees centigrade.

To control the emission wavelength of the device, the laser output should be coupled through a narrowband optical filter so that small wavelengths shifts will be detectable as intensity changes. The detector output should be fed to a control circuit which maintains the diode temperature and the corresponding wavelength in the optical filter passband. Control of the laser wavelength is essential in order to achieve low BER and maintain system performance.

An automatic, periodic channel frequency calibration is also recommended to ensure that channel demultiplexing frequencies are accurate in the presence of temperature variations and potential laser mode hopping.

4.0 Conclusion

The goal of this effort was to evaluate the performance of an optically implemented on-board MCDD that can service inexpensive, low-power earth stations. For such earth stations, no attempt has been made to improve bandwidth efficiency by using advanced modulation and coding schemes. In addition, no effort has been made to minimize ISI by careful design of the earth station transmitter filters. This proof of concept phase has shown that an optically implemented MCDD which promises size, weight and reliability

advantages over other implementations of on-board processors, can perform as well as other implementations with respect to bit error probability.

However, to achieve comparable performance with the optical MCDD, whose transfer function must be carefully controlled, it was found necessary to reduce the ground transmitter filter bandwidths. As seen in Figure 3.1-5, this worsens performance at low signal-to-noise ratios because of the increased ISI that results. The optical MCDD transfer function (Figure 3.1-3) has amplitude and phase characteristics different from most classical filter responses. Also, spurious responses from the reference beams exist. Therefore, the ACI/ISI tradeoff for an optical implementation differs significantly from that for an electronic one.

By using more complicated earth station transmitter filtering, the ISI can be practically eliminated, resulting in greatly improved bit error performance.

References

1. Ananasso, F. and Saggese, E., "A Survey on the Technology of Multicarrier Demodulators for FDMA/TDMA User-oriented Satellite Systems", IEEE International Conference on Communications, Chicago, 1985, pp. 6.6.1 - 6.1.7.

2. Ananasso, F. and Del Re, E., "Clock and Carrier Synchronization in FDMA/TDMA User-oriented Satellite Systems", IEEE International Conference on Communications, Seattle, 1987, pp. 41.7.1 - 41.7.5.

3. Kappes, J. and Sayegh, S., "Programmable Demultiplexer/Demodulator Processor", IEEE Military Communication Conference, Monterey, 1990, pp. 7.3.1 -7.3.5.

4. Goutzoulis, A. and Abramovitz, I., "Digital Electronics Meets Its Match", IEEE Spectrum, Aug. 1988, pp. 21-25.

5. Ananasso, F. and Bennion, I., "Optical Technologies for Signal Processing in Satellite Repeaters", IEEE Communications Magazine, Feb. 1990, pp. 55-64.

REPORT DOCUMENTATION PAGE

Form Approved
OMB No. 0704-0188

1. AGENCY USE ONLY (*Leave blank*)	2. REPORT DATE	3. REPORT TYPE AND DATES COVERED
	January 1994	Final Contractor Report

4. TITLE AND SUBTITLE

Advanced Technology for a Satellite Multichannel Demultiplexer/Demodulator

5. FUNDING NUMBERS

WU-235-01-04
C-NAS3-25865

6. AUTHOR(S)

Irwin J. Abramovitz, Drew E. Flechsig, and Richard M. Matteis, Jr.

7. PERFORMING ORGANIZATION NAME(S) AND ADDRESS(ES)

Westinghouse Electric Corporation
P.O. Box 746, M.S. A255
Baltimore, Maryland 21203

8. PERFORMING ORGANIZATION REPORT NUMBER

E-8317

9. SPONSORING/MONITORING AGENCY NAME(S) AND ADDRESS(ES)

National Aeronautics and Space Administration
Lewis Research Center
Cleveland, Ohio 44135-3191

10. SPONSORING/MONITORING AGENCY REPORT NUMBER

NASA CR-194435

11. SUPPLEMENTARY NOTES

Program Manager, William D. Ivancic, Space Electronics Division, (216) 433-3494.

12a. DISTRIBUTION/AVAILABILITY STATEMENT

Unclassified - Unlimited
Subject Category 17

12b. DISTRIBUTION CODE

13. ABSTRACT (*Maximum 200 words*)

Satellite on-board processing is needed to efficiently service multiple users while at the same time minimizing earth station complexity. The processing satellite receives a wideband uplink at 30 GHz and downconverts it to a suitable Intermediate Frequency. A Multichannel Demultiplexer then separates the composite signal into discrete channels. Each channel is then demodulated by bulk demodulators, with the baseband signals routed to the downlink processor for retransmission to the receiving earth stations. This type of processing circumvents many of the difficulties associated with traditional bent-pipe repeater satellites. Uplink signal distortion and interference are not retransmitted on the downlink. Downlink power can be allocated in accordance with user needs, independent of uplink transmissions. This allows the uplink users to employ different data rates as well as different modulation and coding schemes. In addition, all downlink users have a common frequency standard and symbol clock on the satellite, which is useful for network synchronization in Time Division Multiple Access schemes. The purpose of this program is to demonstrate the concept of an optically implemented Multichannel Demultiplexer (MCD). A Proof-of-Concept (POC) model has been developed which has the ability to receive a 40 MHz wide composite signal consisting of up to 1000 40 kHz QPSK modulated channels and perform the demultiplexing process. In addition a set of Special Test Equipment (STE) has been configured to evaluate the performance of the POC model. The Optical MCD is realized as an acousto-optic spectrum analyzer utilizing the capability of Bragg cells to perform the required channelization. These Bragg cells receive an optical input from a laser source and an RF input (the signal). The Bragg interaction causes optical output diffractions at angles proportional to the RF input frequency. These discrete diffractions are optically detected and output to individual demodulators for baseband conversion. Optimization of the MCD design was conducted in order to achieve a compromise between two opposing sources of signal degradation: Adjacent Channel Interference and Intersymbol Interference. The system was also optimized to allow simple, inexpensive ground stations communications with the MCD. These design goals led to the realization of a POC MCD which demonstrates the demultiplexing function with minimal signal degradation. Performance evaluation results using the STE equipment indicate that the dynamic range of the demultiplexer in the presence of adjacent and multiple channel loading is 40 – 50 dB. Measured Bit Error Rate (BER) probabilities varied from the predicted theoretical results by 1 dB or less. The performance of the Proof-of-Concept model indicate that the development of a space qualified optically implemented MCD are feasible. The advantages to such an implementation include reduced size, weight and power and increased reliability when compared with electronic approaches. All of these factors are critical to on-board satellite processors. Further optimization can be conducted which trade ground station complexity and MCD performance to achieve desired system results.

14. SUBJECT TERMS

Bragg cells; Acousto-optics; Channelizer; Demultiplexer; Demodulator

15. NUMBER OF PAGES
54

16. PRICE CODE
A04

17. SECURITY CLASSIFICATION OF REPORT	18. SECURITY CLASSIFICATION OF THIS PAGE	19. SECURITY CLASSIFICATION OF ABSTRACT	20. LIMITATION OF ABSTRACT
Unclassified	Unclassified	Unclassified	